PHYSICAL REVIEW D **94,** 013014 (2016)

# Nonstandard interactions spoiling the *CP* violation sensitivity at DUNE and other long baseline experiments

Mehedi Masud[1,*] and Poonam Mehta[2,†]

[1]*Harish-Chandra Research Institute, Chhatnag Road, Jhunsi, Allahabad 211 019, India*
[2]*School of Physical Sciences, Jawaharlal Nehru University, New Delhi 110067, India*

(Received 11 March 2016; published 29 July 2016)

It is by now established that neutrino oscillations occur due to nonzero masses and parameters in the leptonic mixing matrix. The extraction of oscillation parameters may be complicated due to subleading effects such as nonstandard neutrino interactions and one needs to have a fresh look how a particular parameter value is inferred from experimental data. In the present work, we focus on an important parameter entering the oscillation framework–the leptonic *CP*-violating phase $\delta$, about which we know very little. We demonstrate that the sensitivity to *CP* violation gets significantly impacted due to nonstandard neutrino interaction effects for the upcoming long baseline experiment, Deep Underground Neutrino Experiment. We also draw a comparison with the sensitivities of other ongoing neutrino beam experiments such as NO$\nu$A and T2K as well as a future generation experiment, T2HK.

DOI: 10.1103/PhysRevD.94.013014

## I. INTRODUCTION

The discovery of neutrino oscillations implies that neutrinos have masses and mix among three active flavors. If neutrinos have masses then the leptonic charged current interactions exhibit mixing and *CP*[1] violation in much the same way as in the quark sector [1,2]. Within the Standard Model (SM), *CP* violation arises naturally via the Dirac phase, $\delta$ in the three flavor case as concocted by Kobayashi and Maskawa [3]. It was suggested [4,5], that a measurement of $\delta$ was possible through neutrino oscillations. The value of $\delta$ could very well be zero, maximal ($\delta \sim \pm\pi/2$) or nonmaximal ($\delta \neq \pm\pi/2$) [6]. The extraction of the value of the *CP* phase is plagued with the matter-induced fake *CP*-violating effects which makes its measurement very challenging even in the case of SM [7,8]. Additionally, we need to know the ordering of the neutrino masses and also the octant of $\theta_{23}$ in order to have a clear understanding of the mixing phenomena.

The Deep Underground Neutrino Experiment (DUNE) is one of the most promising upcoming long baseline experiments that is planned to offer maximal sensitivity to uncover the value of $\delta$ [9–13]. The baseline of 1300 km is expected to deliver optimal sensitivity to *CP* violation and is well suited to address the question of neutrino mass hierarchy [14]. Sensitivity studies leading to optimal configurations have been carried out for DUNE stand alone as well as in conjunction with other long baseline experiments and atmospheric neutrinos and it was shown that the *CP* violation can be established for ∼80% of the *CP* phase values [15,16] (see also [17]) under favorable conditions ($\delta$ around $\pm\pi/2$). Of course, all these studies assume the SM where the only source of *CP* violation is the Dirac *CP* phase. Other interesting proposals to look for leptonic *CP* violation include the proposed Tokai to HyperKamiokande (T2HK) experiment [18] and the MuOn-decay MEdium baseline NeuTrino beam (MOMENT) experiment which exploits neutrinos from muon decay [19].

Since there are clear hints of existence of new physics beyond the SM, it is likely that the SM does not provide a complete description of *CP* violation in nature. A particular new physics scenario would introduce additional sources of *CP*-violating effects in addition to the lone *CP*-violating source ($\delta$) of the SM (see [20,21] for models giving rise to NSI) and this could change the relationship of measured quantities to the *CP*-violating parameter of the SM [22]. In the presence of new physics, we need to reassess the conclusions drawn in connection to *CP* violation. This was discussed in the context of the Neutrino Factory in [23] (see also [24] in context of atmospheric neutrinos) which led to the conclusion that a new physics effect might be misinterpreted as the canonical Dirac *CP* violation or vice-versa. Concerning the value of the *CP* phase $\delta$, there was a mild hint of its value from the global analyses of neutrino data [25] and in recent years, the T2K [26], NO$\nu$A (NuMI off-axis $\nu_e$ Appearance) [27], as well as Super-Kamiokande atmospheric events [28] indicate nearly maximal value ($\delta \sim -\pi/2$) for the *CP* phase although presently the significance of this result is below $3\sigma$. If the significance improves in the future, it is very important to rule out alternative mechanisms such as NSI [29] (also see Refs. [30,31] for reviews and references therein) or *CPT* violation [32,33] or additional sterile neutrinos (see [34,35]) that could very well be consistent with data.

In a recent work [36] (see also [29,37–42]), we studied the impact of flavor diagonal and flavor changing neutral

*masud@hri.res.in
†pm@jnu.ac.in

[1]*CP* stands for charge conjugation and parity discrete symmetry operation.

 

current (NC) nonstandard interactions (NSIs) during propagation on $CP$ measurements at long baselines using DUNE as an example. We discussed the role of individual and collective NSI parameters on the $CP$ measurements. We restricted ourselves to a discussion of $CP$ asymmetries using solely the probability for the electron appearance channel $P_{\mu e}$ and showed how NSI effects translate at the level of event rates. Since then there has been a lot of activity [29,38–42] in this direction exploring effects due to propagation NSI at long baselines. In [38], the goal was to discuss possible improvement of bounds on the NSI parameters using different channels at long baseline experiments. In [39] the correlation between different SI and NSI parameters and ways to distinguish scenarios of new physics (sterile neutrinos versus NSI) compared to the standard case was discussed. In [40], it was shown that new degeneracies in presence of NSI at long baselines can arise which complicate the determination of mass hierarchy, $CP$ violation and octant of $\theta_{23}$. Reference [41] deals with constraining NSI parameters using long baseline experiments. Very recently, it has been suggested that the proposed MOMENT experiment due to its much smaller baseline may prove helpful in solving the degeneracies due to NSIs leading to unambiguous determination of $CP$ violation [42].

While sensitivity studies have been carried out in the presence of NSIs in the context of DUNE, we would like to stress that none of them deal with the precise impact of NSIs on the sensitivity to $CP$ violation at long baseline experiments. We consider NSI terms whose strengths lie in the presently allowed limits (along with the phases associated with these terms which are presently unconstrained) and study the impact of individual and collective NSI terms on the the $CP$ violation sensitivity using different channels. We assess in a comprehensive manner the sensitivity to $CP$ violation offered by present and future generation long baseline experiments: T2K, NO$\nu$A, DUNE, and T2HK when the NSI effects are turned on.

The paper is organized as follows. Section II gives the framework for the present work. Section II A consists of a brief introduction to NSIs in propagation and how the genuine and fake $CP$-violating effects can arise due to NC NSI terms which are constrained. We then discuss the $CP$ dependence of the probabilities $P_{\mu e}$ and $P_{\mu\mu}$ in Sec. II B. In Sec. II C, we give our analysis procedure using the $CP$ dependence of probabilities in Sec. II B. We then go on to describe our results in Sec. III where we show how $CP$ sensitivity at DUNE gets affected due to individual and collective NSI terms (Sec. III A). We also show dependence on true values of standard oscillation parameters in Sec. III B and compare the results obtained at DUNE with other long baseline experiments in Sec. III C. The impact of NSIs on the $CP$ fraction is shown as a function of exposure and baseline in Secs. III D and III E. A discussion of $CP$ violation sensitivity when the source of $CP$ violation is known is given in Sec. III F. Finally, the ability of long baseline experiments to measure the $CP$ phases is discussed in Sec. III G. We conclude with a discussion in Sec. IV.

## II. FRAMEWORK

### A. Genuine and fake $CP$ violation due to Earth matter effects: SI and NSI

It is well known that the three neutrino flavor states can be mapped to a three-level quantum system with distinct energy eigenvalues, $E_i = p + m_i^2/2p$ in the ultrarelativistic limit in vacuum along with the assumption of equal fixed momenta (or energy). In the presence of matter, the relativistic dispersion relation $E_i = f(p, m_i)$ gets modified due to the neutrino matter interactions during propagation. The effective Lagrangian describing the NC-type neutrino NSI of the type $(V-A)(V \pm A)$ is given by

$$\mathcal{L}_{\rm NSI} = -2\sqrt{2} G_F \varepsilon_{\alpha\beta}^{fC} [\bar{\nu}_\alpha \gamma^\mu P_L \nu_\beta][\bar{f}\gamma_\mu P_C f], \qquad (1)$$

where $G_F$ is the Fermi constant, $\nu_\alpha$, $\nu_\beta$ are neutrinos of different flavors, and $f$ is a first generation SM fermion $(e, u, d)$.[2] The chiral projection operators are given by $P_L = (1-\gamma_5)/2$ and $P_C = (1 \pm \gamma_5)/2$. In general, NSI terms can be complex. It should be noted that charged current (CC) NSIs would only affect neutrino production and detection as opposed to NC NSIs and hence as far as propagation of neutrinos is concerned, only the NC NSI is relevant. In the effective Schrödinger equation for neutrino propagation, the effective Hamiltonian in flavor basis is given by

$$\begin{aligned}\mathcal{H}_{\rm f} &= \mathcal{H}_{\rm v} + \mathcal{H}_{\rm SI} + \mathcal{H}_{\rm NSI} \\ &= \lambda \left\{ \mathcal{U} \begin{pmatrix} 0 & & \\ & r_\lambda & \\ & & 1 \end{pmatrix} \mathcal{U}^\dagger + r_A \begin{pmatrix} 1 & 0 & 0 \\ 0 & 0 & 0 \\ 0 & 0 & 0 \end{pmatrix} \right. \\ &\quad \left. + r_A \begin{pmatrix} \varepsilon_{ee} & \varepsilon_{e\mu} & \varepsilon_{e\tau} \\ \varepsilon_{e\mu}^\star & \varepsilon_{\mu\mu} & \varepsilon_{\mu\tau} \\ \varepsilon_{e\tau}^\star & \varepsilon_{\mu\tau}^\star & \varepsilon_{\tau\tau} \end{pmatrix} \right\}, \end{aligned} \qquad (2)$$

where we have used the following ratios:

$$\lambda \equiv \frac{\delta m_{31}^2}{2E}; \qquad r_\lambda \equiv \frac{\delta m_{21}^2}{\delta m_{31}^2}; \qquad r_A \equiv \frac{A(x)}{\delta m_{31}^2} \qquad (3)$$

and the standard CC potential due to the coherent forward scattering of neutrinos is given by $A(x) = 2\sqrt{2} E G_F n_e(x)$ where $n_e$ is the electron number density. $\mathcal{U}$ is the three

[2]Coherence requires that the flavor of the background fermion $(f)$ is preserved in the interaction. Second or third generation fermions do not affect oscillation experiments since matter does not contain them.

flavor neutrino mixing matrix and is responsible for diagonalizing the vacuum part of the Hamiltonian. It is parametrized by three angles $\theta_{12}$, $\theta_{23}$, $\theta_{13}$ and one phase $\delta$

$$\mathcal{U}(\{\theta_{ij}\},\delta) \equiv \mathcal{U}_{23}(\theta_{23}) \cdot \mathcal{W}_{13}(\theta_{13},\delta) \cdot \mathcal{U}_{12}(\theta_{12}) \quad (4)$$

with $\mathcal{W}_{13} = \mathcal{U}_\delta \mathcal{U}_{13} \mathcal{U}_\delta^\dagger$ and $\mathcal{U}_\delta = \mathrm{diag}\{1, 1, \exp(i\delta)\}$].[3] In the commonly used Pontecorvo-Maki-Nakagawa-Sakata parametrization [43], $\mathcal{U}$ is given by

$$\mathcal{U} = \begin{pmatrix} 1 & 0 & 0 \\ 0 & c_{23} & s_{23} \\ 0 & -s_{23} & c_{23} \end{pmatrix} \begin{pmatrix} c_{13} & 0 & s_{13}e^{-i\delta} \\ 0 & 1 & 0 \\ -s_{13}e^{i\delta} & 0 & c_{13} \end{pmatrix} \times \begin{pmatrix} c_{12} & s_{12} & 0 \\ -s_{12} & c_{12} & 0 \\ 0 & 0 & 1 \end{pmatrix}, \quad (5)$$

where $s_{ij} = \sin\theta_{ij}$, $c_{ij} = \cos\theta_{ij}$. If neutrinos are Majorana particles, there can be two additional Majorana-type phases in the three flavor case but they are of no consequence in neutrino oscillations. For the SI case, we note that there is only one parameter, the Dirac *CP* phase $\delta$ that is responsible for genuine *CP* violation while the SI with Earth matter introduces additional fake *CP* effects due to the fact that matter is *CP* asymmetric. This makes it challenging to isolate the value of genuine *CP*-violating phase $\delta$ in the SI case from the fake effects and there are several suggestions to tackle the problem [7,8]. The geometric visualization of *CP* conservation and *CP* violation for the two flavor neutrino case was demonstrated in [44,45].

For the NSI case, the $\varepsilon_{\alpha\beta}(\equiv|\varepsilon_{\alpha\beta}|e^{i\phi_{\alpha\beta}})$ are complex NSI parameters which appear in $\mathcal{H}_{\mathrm{NSI}}$. The diagonal NSI parameters are real due to the Hermiticity of the Hamiltonian. In total, there are four phases appearing in the $\mathcal{H}_{\mathrm{f}}$—one is $\delta$ and the other three are $\varphi_{e\mu}$, $\varphi_{e\tau}$, $\varphi_{\mu\tau}$. The total number of phases is four due to the fact that once we have redefined the phases of the lepton and neutrino wave functions to get $\mathcal{U}$ in form equation (5), the basis of neutrino flavor states is defined fully. The matrix that diagonalizes the NSI part of the Hamiltonian then would require three angles and six phases out of which three are Majorana-type and appear as diagonal matrix. So, we are left with three additional phases that are relevant for us. It may be further possible to reduce the number of phases in the limiting cases such as when $\delta m^2_{21} \to 0$ or $\theta_{12} \to 0$ as a consequence of the phase reduction theorem of Kikuchi *et al.* [46].

For long baseline neutrino experiments, $\sin^2(\lambda L/2) \simeq \mathcal{O}(1)$ which gives

$$\frac{\lambda L}{2} \simeq 1.57 \left[\frac{\delta m^2_{31}}{2.5\times10^{-3}\,\mathrm{eV}^2}\right]\left[\frac{2.5\,\mathrm{GeV}}{E}\right]\left[\frac{L}{1300\,\mathrm{km}}\right] \text{ for DUNE}, \quad (6)$$

for the first oscillation maximum (minimum) in the appearance (disappearance) channel. We note that $E = 1.5$ GeV, $L = 810$ km for NO$\nu$A and $E = 0.6$ GeV, $L = 295$ km for T2K (and also T2HK) also lead to $\lambda L \sim \pi$. Also, $r_A L \sim \mathcal{O}(1)$ for the range of the $E$ and $L$ values considered here.

It is interesting to note that matter (or propagation) NSIs obey unitarity (while source and detector NSIs do not) so effectively we still have an overall unitary matrix that diagonalizes the effective Hamiltonian in the presence of matter NSIs and obeys

$$\sum_i \hat{\mathcal{U}}_{\alpha i}\hat{\mathcal{U}}^\star_{\beta i} = \delta_{\alpha\beta} \quad (7)$$

where $\hat{\mathcal{U}}$ is the unitary matrix that diagonalizes the Hamiltonian in Eq. (2).

$$\mathcal{H}_{\mathrm{d}} = \hat{\mathcal{U}}^\dagger \mathcal{H}_{\mathrm{f}} \hat{\mathcal{U}}, \quad (8)$$

where the elements $\mathcal{H}_{\mathrm{d\,ii}}$ are the eigenvalues of $H_{\mathrm{f}}$.

As far as the constraints on NC NSI parameters are concerned, we refer the reader to Refs. [24,30] for more details. After taking the constraints from neutrino experiments into account, the NSI parameters are constrained as follows:

$$|\varepsilon_{\alpha\beta}| < \begin{pmatrix} 4.2 & 0.3 & 0.5 \\ 0.3 & 0.068 & 0.04 \\ 0.5 & 0.04 & 0.15 \end{pmatrix}. \quad (9)$$

The NSI phases are unconstrained and can lie the allowed range, $\varphi_{\alpha\beta} \in (-\pi, \pi)$ (see Table I).

All the plots presented in this paper are obtained by using the General Long baseline Experiment Simulator and related software [48–51] which numerically solve the full three flavor neutrino propagation equations using the Preliminary Reference Earth Model [52] density profile of the Earth,[4] and the latest values of the neutrino parameters as obtained from global fits [25,55,56]. Unless stated otherwise, we assume normal hierarchy (NH) as the true hierarchy in all the plots.

### B. *CP* phase dependence in $P_{\mu e}$ and $P_{\mu\mu}$

We consider appearance ($\nu_\mu \to \nu_e$) and disappearance ($\nu_\mu \to \nu_\mu$) channels that are relevant in the context of accelerator-based neutrino oscillation experiments

[3]In the general case of $n$ flavors the leptonic mixing matrix $U_{\alpha i}$ depends on $(n-1)(n-2)/2$ Dirac-type *CP*-violating phases. If the neutrinos are Majorana particles, there are $(n-1)$ additional, so-called Majorana-type *CP*-violating phases.

[4]We use the matter density as given by the Preliminary Reference Earth Model. In principle, we can allow for uncertainty in the Earth matter density in our calculations but it would not impact our results drastically [53,54].

TABLE I. SI and NSI parameters used in our study. For the latest global fit to neutrino data see [47].

| Parameter | True Value | Marginalization Range |
|---|---|---|
| SI | | |
| $\theta_{12}$ [deg] | 33.5 | ... |
| $\theta_{13}$ [deg] | 8.5 | ... |
| $\theta_{23}$ [deg] | 45 | ... |
| $\delta m^2_{21}$ [eV$^2$] | $7.5 \times 10^{-5}$ | ... |
| $\delta m^2_{31}$ (NH) [eV$^2$] | $+2.45 \times 10^{-3}$ | ... |
| $\delta m^2_{31}$ (IH) [eV$^2$] | $-2.46 \times 10^{-3}$ | ... |
| $\delta$ | $[-\pi:\pi]$ | $0, \pi$ |
| NSI | | |
| $\varepsilon_{ee}$ | 0.1,0.4,0.7 | [0:1.00] |
| $\varepsilon_{\mu\mu}$ | 0.05 | [0:0.06] |
| $\varepsilon_{\tau\tau}$ | 0.04,0.08,0.12 | [0:0.15] |
| $\lvert\varepsilon_{e\mu}\rvert$ | 0.01,0.04,0.07 | [0:0.10] |
| $\lvert\varepsilon_{e\tau}\rvert$ | 0.01,0.04,0.07 | [0:0.10] |
| $\lvert\varepsilon_{\mu\tau}\rvert$ | 0.01,0.04 | [0:0.04] |
| $\varphi_{e\mu}$ | $[-\pi:\pi]$ | $0, \pi$ |
| $\varphi_{e\tau}$ | $[-\pi:\pi]$ | $0, \pi$ |
| $\varphi_{\mu\tau}$ | $[-\pi:\pi]$ | $0, \pi$ |

considered in the present work. Rather than delving into the detailed expressions, we note that [8,57,58] the oscillation probabilities for different channels can be expressed in terms of the $CP$-even and $CP$-odd terms both in case of vacuum and matter with SI[5] as

(1) $\nu_\mu \to \nu_e$ and $\bar{\nu}_\mu \to \bar{\nu}_e$:

$$P_{\mu e} = a_{\mu e} + b_{\mu e} \sin\delta + c_{\mu e} \cos\delta$$
$$P_{\bar{\mu}\bar{e}} = \bar{a}_{\mu e} - \bar{b}_{\mu e} \sin\delta + \bar{c}_{\mu e} \cos\delta \quad (10)$$

$\delta \to -\delta$ for antineutrinos and the coefficients can be found in Ref. [58]. Thus, $P_{\mu e}$ contains linear polynomials of $\sin\delta$ and $\cos\delta$.

(2) $\nu_\mu \to \nu_\mu$ and $\bar{\nu}_\mu \to \bar{\nu}_\mu$:

$$P_{\mu\mu} \simeq a_{\mu\mu} + c_{\mu\mu} \cos\delta$$
$$P_{\bar{\mu}\bar{\mu}} \simeq \bar{a}_{\mu\mu} + \bar{c}_{\mu\mu} \cos\delta \quad (11)$$

where the $\sin\delta$ term is absent in this case. In addition to the linear polynomials of $\cos\delta$ in this case, there are quadratic terms such as $\cos 2\delta$ (and $\sin 2\delta$) in $P_{\mu\mu}$ for the case of constant or symmetric (asymmetric) matter density profile, but the coefficient of such terms are small in comparison to $a_{\mu\mu}$ and $c_{\mu\mu}$ which is why we do not explicitly mention those here. For antineutrinos, $\delta \to -\delta$ and the coefficients in vacuum and normal matter can be found in Ref. [58].

It is interesting to note that in the presence of matter with SIs, the form of Eqs. (10) and (11) remain intact with the coefficients suitably redefined to account for their dependence on the density of Earth matter. The $CP$-odd and $CP$-even terms in Eqs. (10) and (11) serve as useful guide to measure effects due to $CP$ violation.

Let us now discuss the case of NSIs which is different from SIs in the sense that it not only introduces SI matterlike fake $CP$-violating effects arising from the moduli of the NSI terms but also additional genuine $CP$ phases over and above the SI phase ($\delta$). Of course, the genuine and fake $CP$-violating effects are interrelated. The argument of Kimura *et al.* [57,58] was generalized to the case of NSIs [59,60]. In [59] (for nonzero values of $\varepsilon_{e\tau}$, $\varepsilon_{ee}$, $\varepsilon_{\tau\tau}$), it was shown that the $CP$ dependence of probability given by Eqs. (10) and (11) remains intact even in the presence of NSIs as long as we make appropriate replacement for the effective $CP$-violating phase, $\delta \to \hat{\delta}$.

In Fig. 1, the impact of individual NSI terms on $P_{\mu e}$ and $P_{\mu\mu}$ is shown for the baseline corresponding to DUNE ($L = 1300$ km) at a fixed value of energy $E = 2.5$ GeV. A striking feature can be clearly seen if we compare the nature of the plots on left side versus the right side. We can simplify Eq. (10) to

$$P_{\mu e} = a_{\mu e} - x'_{\mu e} \sin\lambda L/2 \sin\delta + x'_{\mu e} \cos\lambda L/2 \cos\delta$$
$$= a_{\mu e} + x'_{\mu e} \cos(\lambda L/2 + \delta) \quad (12)$$

where $x'_{\mu e}$ can be found in Ref. [61] for SIs. We note that the (first) peak condition for $P_{\mu e}$ is given by $\lambda L/2 \simeq \pi/2$ and therefore for a given $\delta$, the peak (dip) of $P_{\mu e}$ is shifted by an amount $\pi/2$ with respect to $P_{\mu\mu}$ [see Eqs. (11) and (12)]. For SIs, Eq. (10) leads to $P_{\mu e}(0) = a_{\mu e} + c_{\mu e}$ and $P_{\mu e}(\pm\pi) = a_{\mu e} - c_{\mu e}$. From the plot, we see that $P_{\mu e}(0) \sim P_{\mu e}(\pm\pi)$ and this implies that $c_{\mu e} \simeq 0$. Note also that the maxima/minima will be at $\delta = \pm\pi/2$ from Eq. (10). If we keep the relevant NSI phases to zero, the dashed (dotted) curves corresponding to NSIs can go on either side of the solid curve for SIs. For SIs, Eq. (11) leads to $P_{\mu\mu}(0) = a_{\mu\mu} + c_{\mu\mu}$ and $P_{\mu\mu}(\pm\pi) = a_{\mu\mu} - c_{\mu\mu}$. Note also that the maxima/minima will be at $\delta = 0$ or $\pi$ from Eq. (11). For the diagonal parameter $\varepsilon_{ee}$, for both $P_{\mu e}$ and $P_{\mu\mu}$, the effect is like a uniform enhancement (reduction) of the probability values from the SI case depending upon the sign of $\varepsilon_{ee}$.

In Fig. 2, the collective impact of NSI terms is shown for three different experiments at different fixed energies relevant to those experiments. The largest effect of NSI terms can be seen for $P_{\mu e}$ and for DUNE and it diminishes as we go to T2K. For $P_{\mu\mu}$, the effect is similar for all the three experiments so the baseline does not seem to play much role here.

[5]No extra phase, with a suitable redefinition of coefficients.

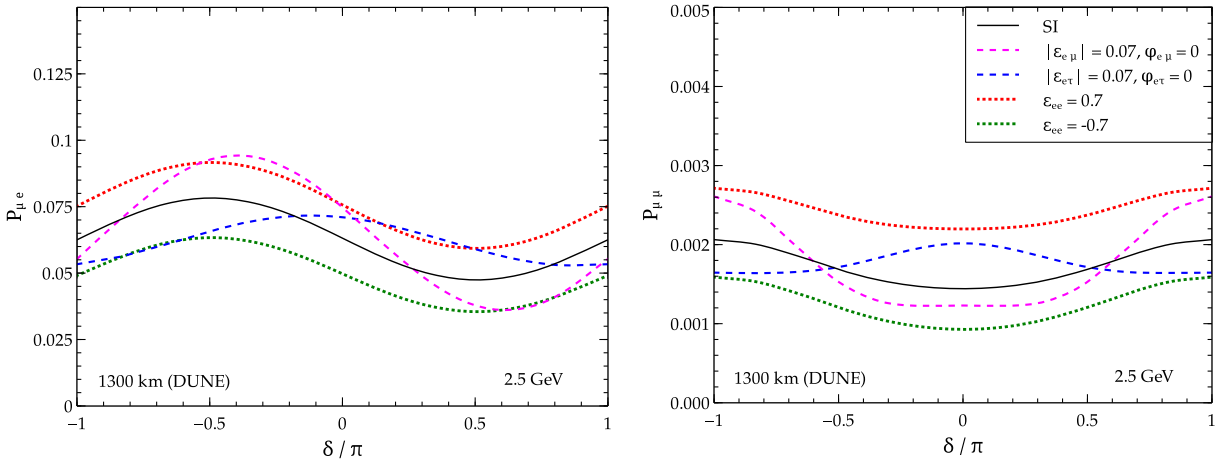


FIG. 1. Effect of individual NSI terms in the $P_{\mu e}$ and $P_{\mu\mu}$ as a function of $\delta$ for $E = 2.5$ GeV and $L = 1300$ km. The solid black curve represents the SI case while the dashed (dotted) curves represent the case of off-diagonal (diagonal) NSI parameters. The NSI phases $\phi_{e\mu}$ and $\phi_{e\tau}$ are set to zero.

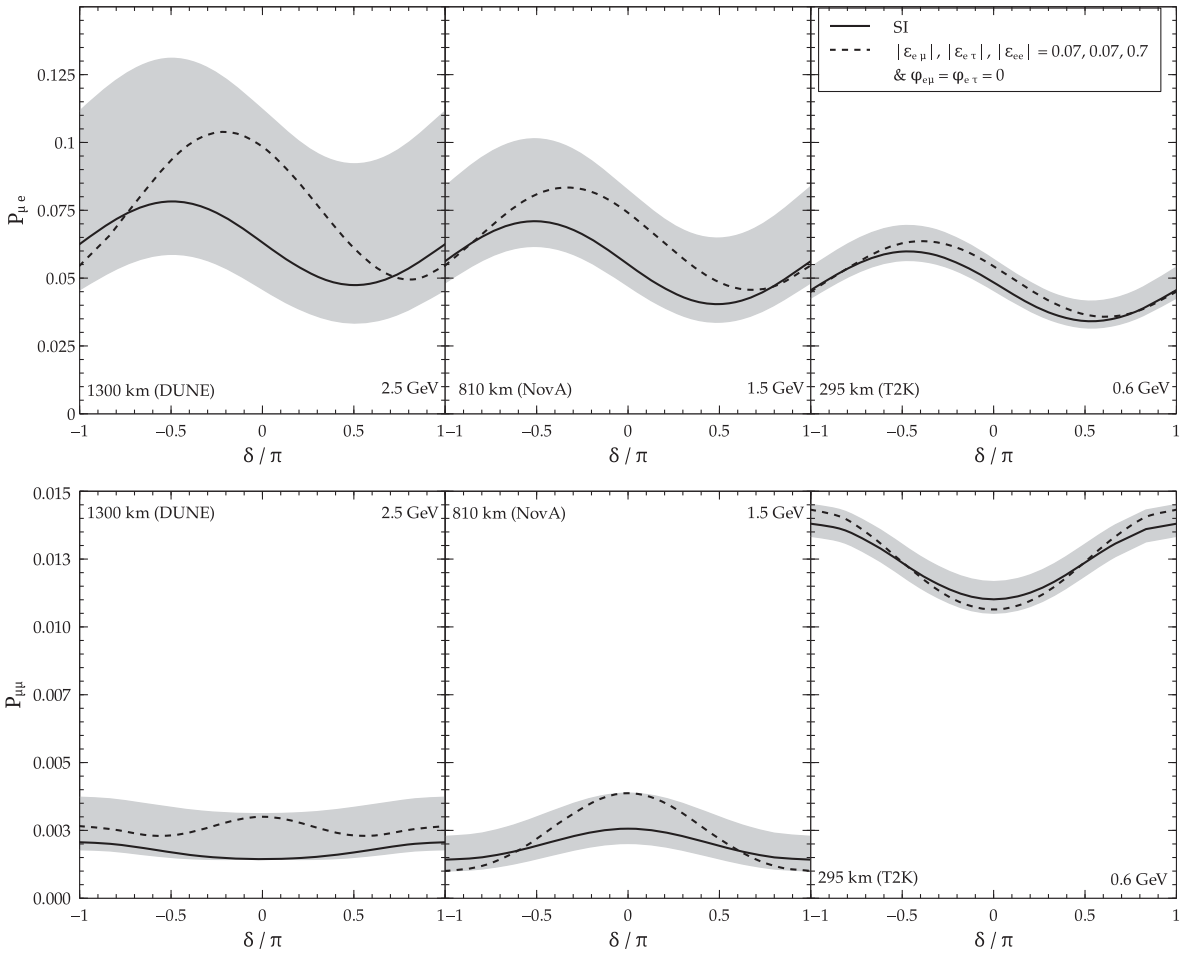


FIG. 2. Combined effect of three NSI terms ($\varepsilon_{e\mu}$, $\varepsilon_{e\tau}$, $\varepsilon_{ee}$) in the electron appearance and muon disappearance probability as a function of $\delta$ (for fixed $E$ and $L$ for DUNE, NO$\nu$A and T2K). The solid black curve represents SIs while the dashed black curve represents NSIs for the particular choice of absolute value of NSI parameters as mentioned in the legend. The grey band shows the spread when, in addition, the NSI phases are varied in the allowed range, i.e., $\phi_{e\mu}$, $\phi_{e\tau} \in [-\pi, \pi]$.

### C. Analysis procedure

In order to obtain the sensitivity to $CP$ violation we need to ask the following question: what is the sensitivity with which a particular experiment can discriminate between $CP$-conserving $(0, \pi)$ and $CP$-violating values $(\neq 0, \pi)$ of the Dirac $CP$ phase $\delta$. In the standard scenario, there is only one $CP$ phase in the neutrino oscillation formalism. However, when we consider NSIs, naturally more parameters in the form of moduli and phases of NSI parameters enter the oscillation formalism which lead to genuine and fake $CP$-violating effects as described above.

For the purpose of understanding the gross features in the plots, we give below the statistical definition of $\chi^2$ for $CP$ violation sensitivity,

$$\chi^2 \equiv \min_{\delta,|\varepsilon|,\varphi} \sum_{i=1}^{x} \sum_{j}^{2} \frac{[N^{i,j}_{\text{true}}(\delta, |\varepsilon|, \varphi) - N^{i,j}_{\text{test}}(\delta = 0, \pi; |\varepsilon|\text{range}; \varphi = 0, \pi)]^2}{N^{i,j}_{\text{true}}(\delta, |\varepsilon|, \varphi)}, \tag{13}$$

where $N^{i,j}_{\text{true}}$ and $N^{i,j}_{\text{test}}$ are the number of true and test events in the $\{i, j\}$th bin, respectively.[6] The NSI parameters are expressed in terms of moduli, $|\varepsilon| \equiv \{|\varepsilon_{\alpha\beta}|; \alpha, \beta = e, \mu, \tau\}$ and phases, $\varphi \equiv \{\varphi_{\alpha\beta}; \alpha, \beta = e, \mu, \tau\}$. The marginalization range of NSI parameters ($|\varepsilon|$range and $\varphi$) and SI parameters ($\delta$) is given in Table I. To determine the $\chi^2$ that represents a particular experiment's sensitivity to the presence of $CP$-violating effects, the test value of phases ($\delta$, $\varphi_{e\mu}$, $\varphi_{e\tau}$) is assumed to be 0 or $\pi$ and the $\chi^2$ for any true value of phase ($\delta$, $\varphi_{e\mu}$, $\varphi_{e\tau}$) in the full range of $[-\pi, \pi]$ is computed.[7] While the variation corresponding to the true value of $\delta$ is depicted along the $x$ axis, the variation of the true values of $\varphi_{e\mu}$, $\varphi_{e\tau}$ (with in the allowed range) lead to the vertical width of the grey bands which show the maximum variation in the $\chi^2$ for each value of $\delta$ (true).[8]

We do not marginalize over the standard oscillation parameters except $\delta$ whose true value is unknown. As we are investigating the role of NSI in the present study, we marginalize over the allowed range of moduli and phases of the relevant NSI parameters. Our choice of range of NSI parameters is consistent with the existing constraints [Eq. (9)].

The indices $i$, $j$ correspond to energy bins ($i = 1 \to x$, the number of bins depends upon the particular experiment —for DUNE, there are $x = 39$ bins of width 250 MeV in 0.5–10 GeV, for T2K and T2HK, there are $x = 20$ bins of width 40 MeV in 0.4–1.2 GeV, for NO$\nu$A, there are $x = 28$ bins of width 125 MeV in 0.5–4 GeV) and the type of neutrinos, i.e., neutrino or antineutrino ($j = 1 \to 2$). As one would expect, the discovery potential of a given experiment vanishes for the $CP$-conserving case ($\delta, \varphi = 0$ or $\pi$). At the values of $\delta$ corresponding to maximum $CP$ violation, i.e., $\delta = \pm\pi/2$, the discovery potential reaches a maximum. So, there is a double peak structure in the sensitivity plot. This can also be understood from the probability curves for the SIs in Figs. 1–2. The appearance probability has a maxima and minima at $\delta = \pm\pi/2$.

For the sake of clarity, we have retained only statistical effects and ignored systematic uncertainties and priors in the above expression (see [16] for the full expression of $\chi^2$ including systematics and priors). However, in our analysis, we have marginalized over systematic uncertainties (see Table II) but assumed that the standard oscillation parameters are known with infinite precision; i.e., we have not included any priors.

The theoretically expected differential event rate is given by [10]

$$\frac{dN^{\text{app}}_{\nu_e}(E, L)}{dE} = N_{\text{target}} \times \Phi_{\nu_\mu}(E, L) \times P_{\mu e}(E, L) \times \sigma_{\nu_e}(E), \tag{14}$$

where $N_{\text{target}}$ is the number of target nucleons per kiloton of detector fiducial volume, $N_{\text{target}} = 6.022 \times 10^{32} N/kt$. $P_{\mu e}(E, L)$ is the appearance probability for $\nu_\mu \to \nu_e$ in matter, $\Phi_{\nu_\mu}(E, L)$ is the flux of $\nu_\mu$, $\sigma_{\nu_e}(E)$ is the CC cross section of $\nu_e$ given by

$$\sigma_{\nu_e} = 0.67 \times 10^{-42} (m^2/\text{GeV}/N) \times E, \quad \text{for } E > 0.5\,\text{GeV}. \tag{15}$$

For the disappearance channel, $P_{\mu e}$ is to be replaced by $P_{\mu\mu}$ and $\sigma_{\nu_e} \to \sigma_{\nu_\mu}$. Note that $\sigma_{\nu_\mu} \sim \sigma_{\nu_e}$ for the considered energy range. For antineutrinos, $\nu_\mu \to \bar{\nu}_\mu$ and $\nu_e \to \bar{\nu}_e$ and $P_{\mu e} \to \bar{P}_{\mu e}$.

The $\chi^2$ for the appearance channel is obtained by adding the neutrino ($\nu_\mu \to \nu_e$) and antineutrino ($\bar{\nu}_\mu \to \bar{\nu}_e$) contributions,[9] which gives

[6] $N_\sigma = \sqrt{\Delta\chi^2}$. $\Delta\chi^2 = \chi^2$ as we have not included any fluctuations in simulated data. This is the Pearson's definition of $\chi^2$ [62]. For a large sample size, the other definition using log-likelihood also yields similar results.

[7] $\delta$, $\varphi_{e\mu}$, $\varphi_{e\tau}$ can take 0, $\pi$ and there there are eight possibilities for $CP$ conservation in NSI case as opposed to two in the SI case.

[8] The true values of $\varphi_{e\mu}$ and $\varphi_{e\tau}$ that lead to maximum and minimum $\chi^2$ are, in general, not the same for each $\delta$ (true).

[9] Note that the factors such as $N_{\text{target}}$, $\Phi_{\nu_\mu}$ ($\bar{\Phi}_{\nu_\mu}$), and $\sigma_{\nu_\mu/\nu_e}$ ($\sigma_{\bar{\nu}_\mu/\bar{\nu}_e}$) will also be present, but they are independent of the $CP$ phase and hence omitted in the discussion that follows.

TABLE II. Detector configuration, efficiencies, resolutions and systematic uncertainties for DUNE, NO$\nu$A, T2K, and T2HK.

| | Normalization Error | | Energy Calibration Error | |
|---|---|---|---|---|
| Detector Details | Signal | Background | Signal | Background |
| DUNE | | | | |
| Runtime (yr) $= 5\nu + 5\bar{\nu}$ | $\nu_e$:5% | $\nu_e$:10% | $\nu_e$:2% | $\nu_e$:10% |
| 35 kton, LArTPC | | | | |
| $\varepsilon_{\rm app} = 80\%$, $\varepsilon_{\rm dis} = 85\%$ | $\nu_\mu$:5% | $\nu_\mu$:10% | $\nu_\mu$:5% | $\nu_\mu$:10% |
| $R_\mu = 0.20/\sqrt{E}$, $R_e = 0.15/\sqrt{E}$ | | | | |
| NO$\nu$A | | | | |
| Runtime (yr) $= 3\nu + 3\bar{\nu}$ | $\nu_e$:5% | $\nu_e$:10% | $\nu_e$:0.01% | $\nu_e$:0.01% |
| 14 kton, TASD | | | | |
| $\varepsilon_{\rm app} = 55\%$, $\varepsilon_{\rm dis} = 85\%$ | $\nu_\mu$:2.5% | $\nu_\mu$:10% | $\nu_\mu$:0.01% | $\nu_\mu$:0.01% |
| $R_\mu = 0.06/\sqrt{E}$, $R_e = 0.085/\sqrt{E}$ | | | | |
| T2K | | | | |
| Runtime (yr) $= 3\nu + 3\bar{\nu}$ | $\nu_e$:5% | $\nu_e$:5% | $\nu_e$:0.01% | $\nu_e$:0.01% |
| 22.5 kton, WC | | | | |
| $\varepsilon_{\rm app} = 50\%$, $\varepsilon_{\rm dis} = 90\%$ | $\nu_\mu$:2.5% | $\nu_\mu$:20% | $\nu_\mu$:0.01% | $\nu_\mu$:0.01% |
| $R_\mu = 0.085/\sqrt{E}$, | | | | |
| $R_e = 0.085/\sqrt{E}$ | | | | |
| T2HK | | | | |
| Runtime (yr) $= 1\nu + 3\bar{\nu}$ | $\nu_e$:5% | $\nu_e$:5% | $\nu_e$:0.01% | $\nu_e$:0.01% |
| 560 kton, WC | | | | |
| $\varepsilon_{\rm app} = 50\%$, $\varepsilon_{\rm dis} = 90\%$ | $\nu_\mu$:2.5% | $\nu_\mu$:20% | $\nu_\mu$:0.01% | $\nu_\mu$:0.01% |
| $R_\mu = 0.085/\sqrt{E}$, $R_e = 0.085/\sqrt{E}$ | | | | |

$$\begin{aligned}\chi^2_{\rm app} &= \chi^2_{\nu_\mu\to\nu_e} + \chi^2_{\bar{\nu}_\mu\to\bar{\nu}_e},\\ &\propto \min_{0,\pi}\{[P^{\rm true}_{\mu e} - P^{\rm test}_{\mu e}]^2 + [\bar{P}^{\rm true}_{\mu e} - \bar{P}^{\rm test}_{\mu e}]^2\},\\ &= \min_{0,\pi}\{[b_{\mu e}\sin\delta_{\rm true} + c_{\mu e}\cos\delta_{\rm true} - c_{\mu e}\cos\delta|_{0,\pi}]^2\\ &\quad + [-\bar{b}_{\mu e}\sin\delta_{\rm true} + \bar{c}_{\mu e}\cos\delta_{\rm true} - \bar{c}_{\mu e}\cos\delta|_{0,\pi}]^2\}.\end{aligned} \tag{16}$$

Here the $\sin\delta_{\rm test}$ term vanishes while $\cos\delta_{\rm test}$ does not for the two *CP*-conserving values $\delta = 0, \pi$. Similarly, the $\chi^2$ for the disappearance channel is obtained by adding the neutrino ($\nu_\mu \to \nu_\mu$) and antineutrino ($\bar{\nu}_\mu \to \bar{\nu}_\mu$) contributions,

$$\begin{aligned}\chi^2_{\rm dis} &= \chi^2_{\nu_\mu\to\nu_\mu} + \chi^2_{\bar{\nu}_\mu\to\bar{\nu}_\mu},\\ &\propto [P^{\rm true}_{\mu\mu} - P^{\rm test}_{\mu\mu}]^2 - [P^{\rm true}_{\bar{\mu}\bar{\mu}} - P^{\rm test}_{\bar{\mu}\bar{\mu}}]^2,\\ &= \min_{0,\pi}\{[c_{\mu\mu}\cos\delta_{\rm true} - c_{\mu\mu}\cos\delta|_{0,\pi}]^2\\ &\quad + [\bar{c}_{\mu\mu}\cos\delta_{\rm true} - \bar{c}_{\mu\mu}\cos\delta|_{0,\pi}]^2\}.\end{aligned} \tag{17}$$

Note that both $\chi^2_{\rm app}$ and $\chi^2_{\rm dis}$ depend on $\cos\delta_{\rm true}$ while $\chi^2_{\rm app}$ also depends on $\sin\delta_{\rm true}$. The presence of the $\sin\delta_{\rm true}$ term in the $\chi^2_{\rm app}$ ensures that the appearance channel contributes dominantly to the *CP* violation sensitivity. The total $\chi^2$ when appearance and disappearance channels are combined is given by

$$\begin{aligned}\chi^2_{\rm tot} &\propto \min_{0,\pi}\{[b_{\mu e}\sin\delta_{\rm true} + c_{\mu e}\cos\delta_{\rm true} - c_{\mu e}\cos\delta|_{0,\pi}]^2\\ &\quad + [-\bar{b}_{\mu e}\sin\delta_{\rm true} + \bar{c}_{\mu e}\cos\delta_{\rm true} - \bar{c}_{\mu e}\cos\delta|_{0,\pi}]^2\\ &\quad + [c_{\mu\mu}\cos\delta_{\rm true} - c_{\mu\mu}\cos\delta|_{0,\pi}]^2\\ &\quad + [\bar{c}_{\mu\mu}\cos\delta_{\rm true} - \bar{c}_{\mu\mu}\cos\delta|_{0,\pi}]^2\}.\end{aligned} \tag{18}$$

In order to quantify the effects due to *CP* violation, another quantity called a *CP* fraction $f(\sigma > 3)$ is often used. This refers to the fraction of $\delta$ values for which *CP* violation can be determined above a particular value of significance (here, $3\sigma$). Being a fraction, $f(\sigma > 3)$ naturally lies between 0 and 1.

## III. RESULTS

### A. *CP* sensitivity: Impact of individual and collective NSI terms at DUNE

In order to clearly understand the impact of the NSI terms, we first take only one parameter nonzero at a time. We show the effect of that particular parameter on *CP* sensitivity in the appearance ($\nu_\mu \to \nu_e$) as well as the disappearance ($\nu_\mu \to \nu_\mu$) channels. We also show the case with the two channels combined.

Before we describe the impact of a particular NSI parameter (i.e., $\varepsilon_{e\mu}$) we would like to point out that there are two effects responsible for altering the value of the $\chi^2$ which compete with each other. In general, we first note that the NSI introduces more numbers of parameters (in the

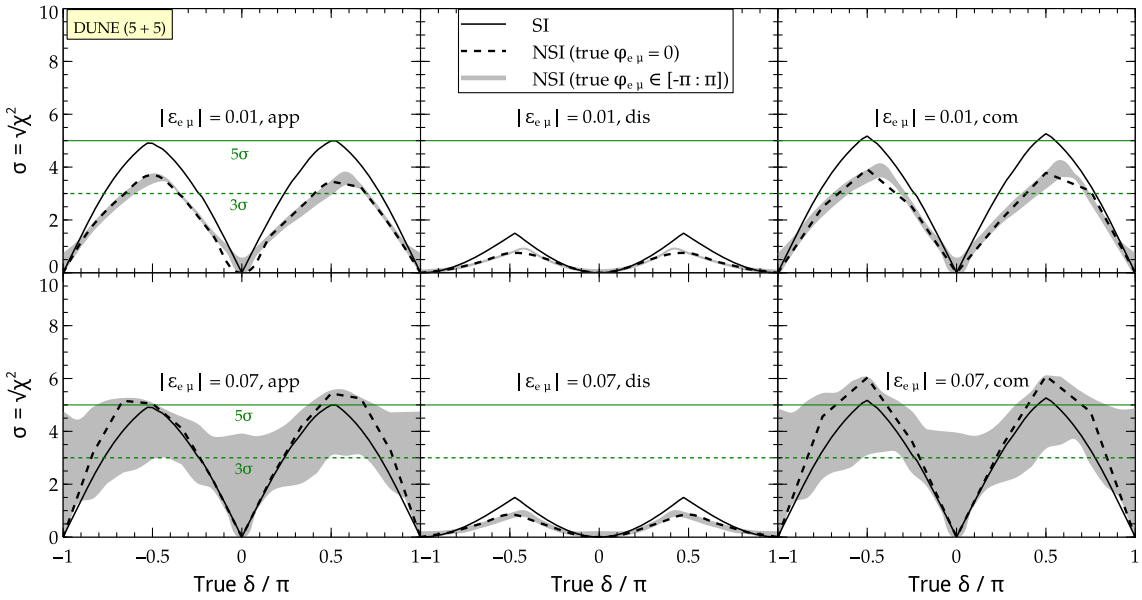


FIG. 3. The impact of $\varepsilon_{e\mu}$ on the significance with which the $CP$ violation can be determined as a function of the value of $\delta$ at DUNE for an exposure of 350 kt. MW. yr assuming NH. The solid black curve represents the sensitivity for our reference design. Both the moduli and phases are varied as mentioned in the legend. The appearance and disappearance channels are shown separately and the sensitivity obtained by combining both the channels is also shown in the last column.

form of moduli of NSI terms and the associated $CP$ phases) in the sensitivity analysis and also introduces more sources of $CP$ violation. One can have the following possibilities:

(a) Decrease in $\chi^2$ due to additional test values: If marginalization is carried out over more numbers of test parameters, it naturally results in a decreased value of $\chi^2$. This is purely a statistical effect.

(b) Increase in $\chi^2$ due to the larger strength of true values: In addition to more parameters in the test data set [as mentioned in effect (a) above], one has to deal with a larger set of parameters in the true data set as well. The variation over the values of the true NSI phases ($\varphi_{e\mu}$ or $\varphi_{e\tau}$) tends to broaden the grey band provided the true value of the moduli ($|\varepsilon_{e\mu}|$ or $|\varepsilon_{e\tau}|$) of the relevant NSI term is large.

In Fig. 3, we show the sensitivity to $CP$ violation by exploiting appearance and disappearance channels (in isolation and combined) for the off-diagonal NSI parameter, $\varepsilon_{e\mu}$ and compare it with the sensitivity obtained in case of SIs as a benchmark. The $3\sigma$ ($5\sigma$) value is shown as a horizontal green dashed (solid) line to serve as a reference. Let us first describe the SI case (shown as solid black curves). The $P_{\mu e}$ channel dominates the sensitivity of $CP$ violation which can be understood from the presence of the $CP$-odd term. The mild $CP$ sensitivity of the $P_{\mu\mu}$ (due to the presence of $CP$-even terms and absence of $CP$-odd terms in $P_{\mu\mu}$) is not useful when considered in isolation but improves the $\chi^2$ in the combined case. The maximum (minimum) sensitivity in the case of SIs is attained when $\delta \simeq \pm\pi/2$ ($\delta = 0, \pm\pi$). In presence of NSIs, in general, the maximum $\chi^2$ is shifted from the SI maximum, $\delta = \pm\pi/2$. This is due to the shift in the position of peaks and dips from the SI curve at the level of probability as mentioned in Sec. II B.

In $P_{\mu e}$, the presence of additional $CP$-odd ($\sin\delta$-like) terms in the presence of NSIs makes it possible for effect (b) to overtake (a) if the value of the NSI parameter is large enough. If we see the top row of Fig. 3, the value of NSI parameter is small (true $|\varepsilon_{e\mu}| = 0.01$) and the black dashed curve (true $|\varepsilon_{e\mu}| \neq 0$) and the grey band (true $|\varepsilon_{e\mu}| \neq 0$, $\varphi_{e\mu} \in [\pi : \pi]$) are always below the SI case due to dominant (a) above. But for true $|\varepsilon_{e\mu}| = 0.07$, effect (b) becomes larger than effect (a) and we note that the NSI (with $|\varepsilon_{e\mu}| \neq 0$) overtakes the SI. Also, the grey band spreads around the SI curve. The most surprising outcome is that there can be $\geq 3\sigma$ sensitivity to $CP$ violation even when $\delta = 0, \pm\pi$ (SI, $CP$ conservation) for some (un)favorable choice of NSI moduli and phases. We can see this in the bottom panel of the left and right plots of Fig. 3. As can be seen from the middle plots in the top and bottom rows of Fig. 3 corresponding to $P_{\mu\mu}$, such an overtaking is not possible due to the absence of $CP$-odd terms (unless $CPT$ is violated) which forbids (b) to overtake (a) and there is always a net reduction in $\chi^2$ due to (a) even if the NSI parameter is large.

In Fig. 4, the combined (appearance + disappearance) sensitivity to $CP$ violation is shown both for SI and when the NSI parameter $\varepsilon_{e\tau}$ is incorporated. The effects are comparable in strength and similar in nature to that of $\varepsilon_{e\mu}$ described above. The impact of the off-diagonal NSI

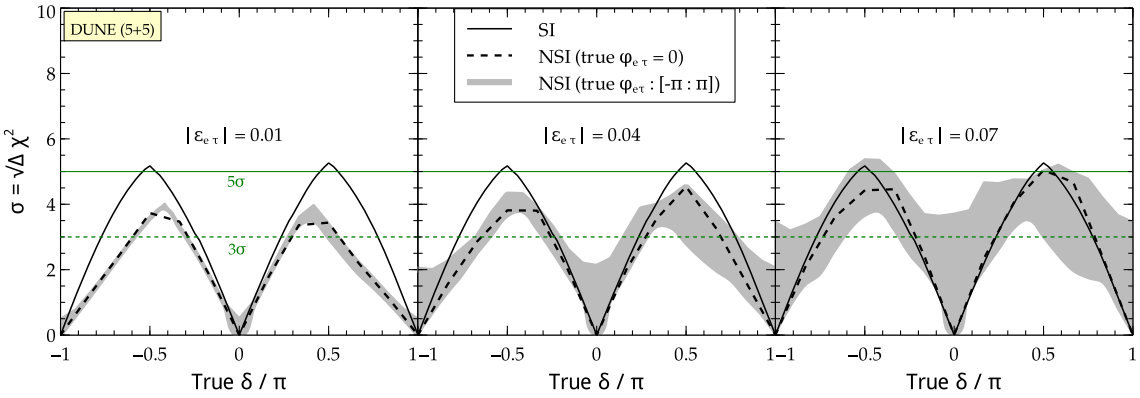


FIG. 4. The impact of $\varepsilon_{e\tau}$ on the significance with which the *CP* violation can be determined as a function of the value of $\delta$ at DUNE for an exposure of 350 kt. MW. yr assuming NH. The solid black curve represents the sensitivity for reference design. Both the moduli and phases are varied as mentioned in the legend. The combined sensitivity of appearance and disappearance channels is shown in the plot.

parameter $\varepsilon_{\mu\tau}$ on the *CP* sensitivity is found to be negligible even if we choose values close to the upper limit mentioned in Eq. (9) and hence, is not shown here.

Having described the effect of off-diagonal NSI terms, we now address the impact of the diagonal ones: $\varepsilon_{ee}$, $\varepsilon_{\mu\mu}$, $\varepsilon_{\tau\tau}$. We show the impact of the three diagonal NSI parameters ($\varepsilon_{ee}$, $\varepsilon_{\mu\mu}$, and $\varepsilon_{\tau\tau}$) in Fig. 5. The effect of $\varepsilon_{\mu\mu}$ is very small as it is the most constrained parameter [Eq. (9)]. For the choice of values of the NSI parameters, the *CP* sensitivity sees a drop most likely due to the statistical effect (a) dominating in these cases.

After understanding the impact of individual diagonal as well as off-diagonal NSI terms, we now address the collective effect of the most influential NSI terms as far as *CP* sensitivity is concerned. In Fig. 6, we show the collective impact of the three terms ($|\varepsilon_{ee}|$, $|\varepsilon_{e\mu}|$, $|\varepsilon_{e\tau}|$) which show the largest impact when considered in isolation. We note that when the NSI terms are small, the associated phases of the NSI terms (even if taken collectively) do not contribute in an observable manner to (b) and (a) dominates. However, when we take somewhat larger values, we see the interplay of the two effects (a) and (b) with the possibility of the second effect (b) overtaking the first (a) as we go from small to large values keeping the marginalization range intact.

We summarize the impact of NSI on the *CP* violation sensitivity at long baselines as shown in Fig. 6 for DUNE. If we compare the solid and dashed black curves, we note that for small values of parameters (0.01,0.01,0.1) NSI brings down the $\chi^2$ from $\sim 5\sigma$ to $\sim 3\sigma$ at $\delta \sim \pm\pi/2$ for the case of zero NSI phases. The impact of true nonzero NSI phases can be seen in the form of grey bands for the choice of moduli of the NSI terms. For larger values of parameters (0.07,0.07,0.7) NSI can drastically alter the $\chi^2$ not only at $\delta \simeq \pm\pi/2$ (SI, maximum) but at almost all values of $\delta$ including at $\delta = 0, \pm\pi$ if we allow for phase variation. For some particular choice of the NSI moduli and phases, we note that in this case, the $\chi^2$ decreases from $\sim 5\sigma$ to $\sim 2.5\sigma$ or increases to $\gtrsim 5.5\sigma$ not only at $\delta \simeq \pm\pi/2$ but for most values of $\delta$. This can lead to a misleading inference that *CP* is violated even when we have *CP* conservation in the SI case ($\delta = 0, \pm\pi$). Here the phases have a bigger impact

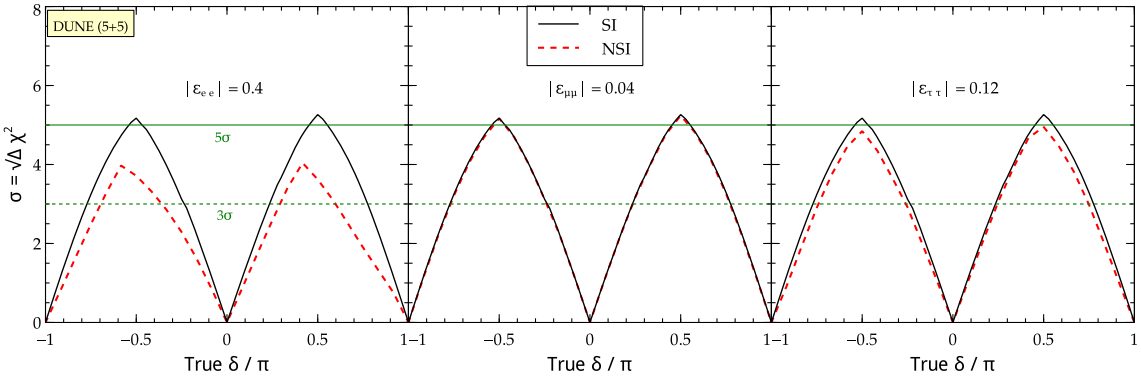


FIG. 5. The impact of $|\varepsilon_{ee}|$, $|\varepsilon_{\mu\mu}|$ and $|\varepsilon_{\tau\tau}|$ on the significance with which the *CP* violation can be determined as a function of the true value of $\delta$ at DUNE for an exposure of 350 kt. MW. yr assuming NH. The solid black curve represents the SI sensitivity for our reference design. The sensitivity obtained by combining the appearance and disappearance channels is shown.

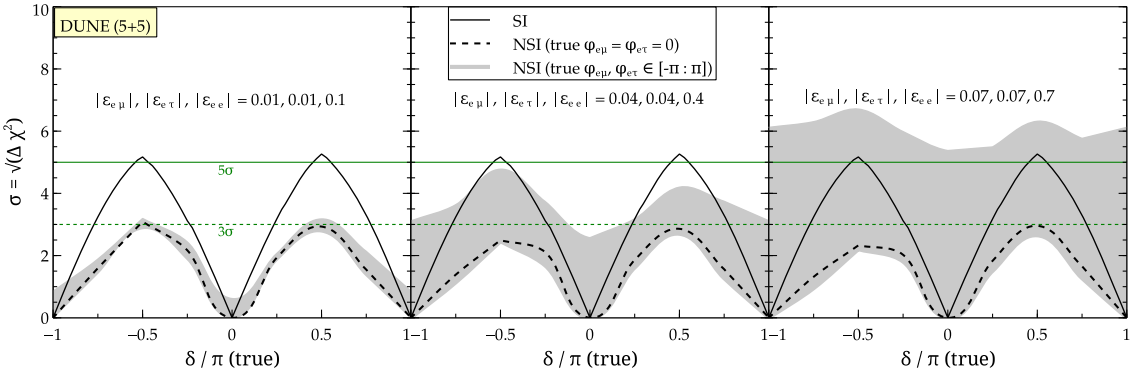


FIG. 6. *CP* sensitivity for collective NSI terms at DUNE.

which can be seen as a widening of the grey bands as we go from smaller to larger moduli of NSI terms.

### B. Dependence on $\theta_{23}$ and $\delta m^2_{31}$

The variation in *CP* sensitivity due to different values of $\theta_{23}$ and $\delta m^2_{31}$ in the allowed range is shown in Fig. 7 for SI and NSI cases (zero NSI phases). For $\theta_{23}$, as can be seen from the solid curves for SI, the significance (the in presence of diagonal and off-diagonal NSI) decreases almost uniformly for all values of $\delta$ as $\theta_{23}$ becomes larger. This can be understood from Eqs. (10) [58] and (13). The $P_{\mu e}$ increases with $\theta_{23}$ and therefore the $\chi^2$ decreases. For no extra phases, we expect the sensitivity in the presence of NSI to be lower than the SI case due to the statistical effect.

For $\delta m^2_{31}$, the solid curves for SI show that the significance does not change significantly for all values of $\delta_{CP}$ as $\delta m^2_{31}$ is varied. Once again this can be understood from Eqs. (10) [58] and (13). The true value of $\delta m^2_{31}$ does not impact $P_{\mu e}$ and therefore the $\chi^2$ remains almost the same.

### C. Comparison with other experiments

We now discuss how various currently running and future experiments will aid in determining the *CP* violation sensitivity in conjunction with DUNE or in isolation. Before we go on, we give a brief description of the experiments that are sensitive to the appearance ($\nu_\mu \to \nu_e$) channel as well as the disappearance ($\nu_\mu \to \nu_\mu$) channel.

T2K: The T2K experiment has a baseline of 295 km and the detector is placed at an off-axis (2.5 degrees) location. An intense beam of neutrinos (mainly $\nu_\mu$ or $\bar{\nu}_\mu$) produced in the J-PARC accelerator facility in Tokai are directed towards the Super-Kamiokande detector (22.5 kton fiducial mass) situated in Kamioka. The near detectors located

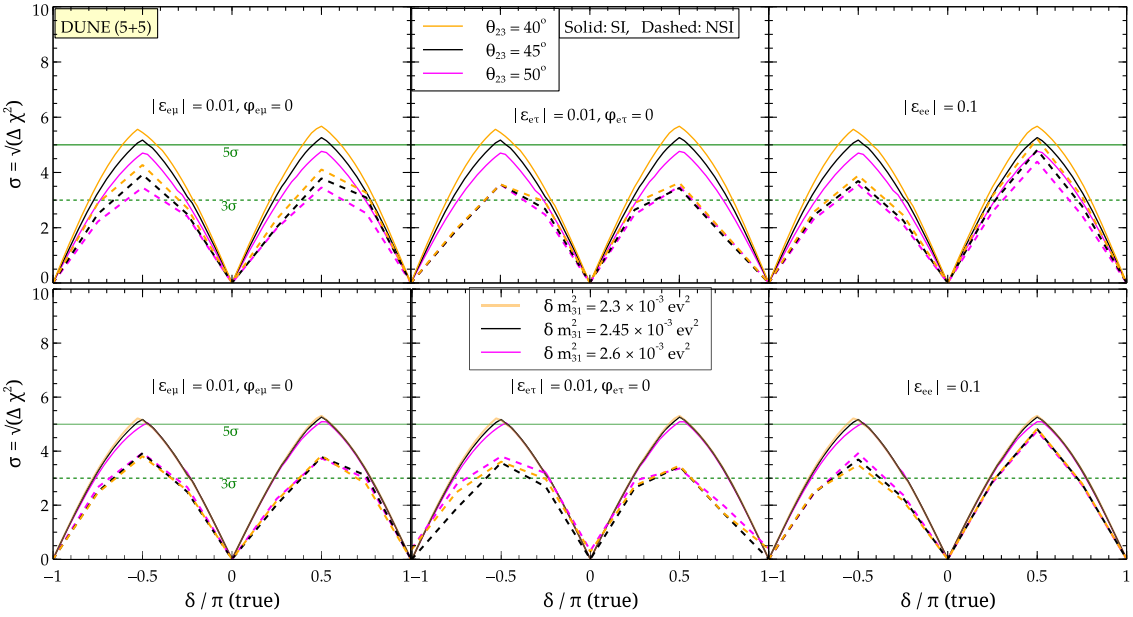


FIG. 7. The dependence of *CP* sensitivity on the value of $\theta_{23}$ and $\delta m^2_{31}$ varied in the allowed range. The black curve is for $\theta_{23} = 45$ deg and for our reference setup (provides a significance of at least $3\sigma$ for ~55% of $\delta$ values).

TABLE III. Total number of signal events (SI/NSI) summed over all energy bins for each experiment using the oscillation parameters given in Table I. For NSI, we show the collective case when the NSI parameters $|\varepsilon_{e\mu}| = 0.07$, $|\varepsilon_{e\tau}| = 0.07$, $|\varepsilon_{ee}| = 0.7$, $\varphi_{e\mu} = 0$ and $\varphi_{e\tau} = 0$ are considered.

| | Appearance Channel | | Disappearance Channel | |
|---|---|---|---|---|
| Experiment | $\nu_\mu \to \nu_e$ | $\bar{\nu}_\mu \to \bar{\nu}_e$ | $\nu_\mu \to \nu_\mu$ | $\bar{\nu}_\mu \to \bar{\nu}_\mu$ |
| DUNE | | | | |
| $\delta = -\pi/2$ | 1610/1779 | 229/214 | 11431/11418 | 7841/7840 |
| $\delta = 0$ | 1350/1803 | 292/257 | 11401/11313 | 7805/7826 |
| $\delta = \pi/2$ | 1028/1182 | 309/279 | 11431/11417 | 7841/7840 |
| NO$\nu$A | | | | |
| $\delta = -\pi/2$ | 90/95 | 17/15 | 142/143 | 46/47 |
| $\delta = 0$ | 78/93 | 25/20 | 141/140 | 45/46 |
| $\delta = \pi/2$ | 57/62 | 30/27 | 142/143 | 46/47 |
| T2K | | | | |
| $\delta = -\pi/2$ | 127/130 | 20/19 | 372/371 | 130/129 |
| $\delta = 0$ | 111/119 | 29/27 | 367/365 | 127/128 |
| $\delta = \pi/2$ | 80/82 | 33/32 | 372/371 | 130/129 |
| T2HK | | | | |
| $\delta = -\pi/2$ | 10231/10490 | 4882/4708 | 30048/30041 | 31321/31334 |
| $\delta = 0$ | 8979/9631 | 6989/6474 | 29641/29515 | 30920/31059 |
| $\delta = \pi/2$ | 6431/6643 | 7962/7737 | 30048/30041 | 31321/31334 |

280 m away from the point of neutrino production are used to monitor the neutrino flux. The $\nu_\mu$ beam peaks at $E \sim 0.6$ GeV which is close to the first oscillation maximum of $P_{\mu e}$. The proton beam power is 770 kW with proton energy of 50 GeV for 3 yr (in $\nu$ mode) +3 yr (in $\bar{\nu}$ mode) which corresponds to a total exposure of $8.3 \times 10^{20}$ protons on target (p.o.t) per year.

NO$\nu$A: The NO$\nu$A experiment has a baseline of 810 km and the detector is placed at an off-axis (0.8 degrees) location. An intense beam of neutrinos (mainly $\nu_\mu$ or $\bar{\nu}_\mu$) produced by firing protons from the FermiLab Main Injector on a graphite target. A $\nu_\mu(\bar{\nu}_\mu)$ beam line is directed towards a Totally Active Scintillator Detector (TASD) of fiducial mass 14 kton placed in Ash River, Minnesota. This off-axis narrow-width beam peaks at ~1.6 GeV which is the energy at which $\nu_\mu \to \nu_e$ oscillation sees a maximum. A 0.3 kton near detector is located at the FermiLab site to monitor the unoscillated neutrino flux. The experiment will be running in $\nu$ mode for 3 years and $\bar{\nu}$ mode for 3 years with a NuMI beam power of 0.7 MW and 120 GeV proton energy, corresponding to $6.0 \times 10^{20}$ p.o.t per year.

DUNE: The DUNE experiment has a baseline of 1300 km and the detector is placed at an on-axis location. A new, high intensity, neutrino beam will be directed towards a LArTPC located at Homestake at a distance of 1300 km. The $\nu_\mu$ beam peaks at $E \sim 2.5$ GeV which is close to the first oscillation maximum of $P_{\mu e}$. This facility is designed for operation at a proton beam power of 1.0 MW, with the proton energy of 120 GeV that will deliver $10^{21}$ p.o.t. in ~200 days per calendar year. To have the LArTPC cross sections, we have scaled the inclusive charged current cross sections of water by 1.06(0.94) for the $\nu(\bar{\nu})$ case.

T2HK: The T2HK experiment has a baseline of 295 km and the detector is placed at the same off-axis (0.8 degrees) location as in T2K. The idea is to upgrade the T2K experiment, with a much larger detector (560 kton fiducial mass) located in Kamioka so that much larger statistics is ensured. T2HK will run for 1 yr (in $\nu$ mode) +3 yr (in $\bar{\nu}$ mode). The proton beam power is 7.5 MW with proton energy of 30 GeV that will deliver $1.6 \times 10^{22}$ p.o.t. per year.

The detailed detector characteristics and systematic errors are listed in Table II. In Table III, we list the energy integrated events[10] for the four experiments (using appearance and disappearance channels) for neutrinos as well as antineutrinos for NH. One striking feature to note is that the events in the disappearance channel are much larger than in the appearance channel. This is due to the fact that the maximum value that $P_{\mu\mu}$ takes is close to 1 while $P_{\mu e}$ at best goes up to ~0.1. The larger detector size of T2K compensates for the shorter baseline when compared to the smaller detector of NO$\nu$A with a longer baseline and the event rates

[10]The energy range for the various experiments is mentioned in Sec. II C.

for the two experiments are comparable. The event rates are somewhat larger for DUNE as it has a bigger detector in comparison to NO$\nu$A. But, T2HK with its massive detector overcomes the limitation of baseline being short and gives the maximum number of events.

The expected sensitivity offered by different experiments (singly or combined) is illustrated in Figs. 6, 8, and 9. Figure 6 shows the *CP* violation sensitivity for DUNE. In Fig. 8, we show the *CP* sensitivity for T2K, NO$\nu$A, and a combination of T2K, NO$\nu$A, and DUNE. Finally, we show the *CP* violation sensitivity for T2HK in Fig. 9 which is competitive with DUNE.

We have shown the *CP* violation sensitivity at DUNE in Fig. 6 and discussed the features in Sec. III A. In Fig. 8, we show the *CP* sensitivity for T2K (top row), NO$\nu$A (middle row) as well as a combination of T2K, NO$\nu$A, and DUNE (bottom row). As in Fig. 6, the characteristic double peak is seen for all the three cases in Fig. 8. If we now look at T2K and NO$\nu$A individually, we note that the *CP* violation sensitivity almost never reaches $3\sigma$ [it barely touches $\sim 1.6\sigma$ (for T2K) and $\sim 1.8\sigma$ (for NO$\nu$A)]. This means that these two current experiments considered in isolation are not so interesting as far as *CP* violation sensitivity is concerned. This does not come as a surprise as these are not optimized for *CP* sensitivity. However, if we combine data from these two experiments with DUNE, we note that *CP* violation sensitivity improves slightly (from $\sim 5.1\sigma$ to $\sim 5.6\sigma$ in the SI case near the peak). For NSI (zero NSI phases, dashed black curve) it improves marginally from $\sim 3\sigma$ to $\gtrsim 3\sigma$. In general, we note that if the phases are taken into account, the grey bands expand and even out as we go from small to large NSI, the peaks at $\delta \sim \pm\pi/2$ smoothen out which

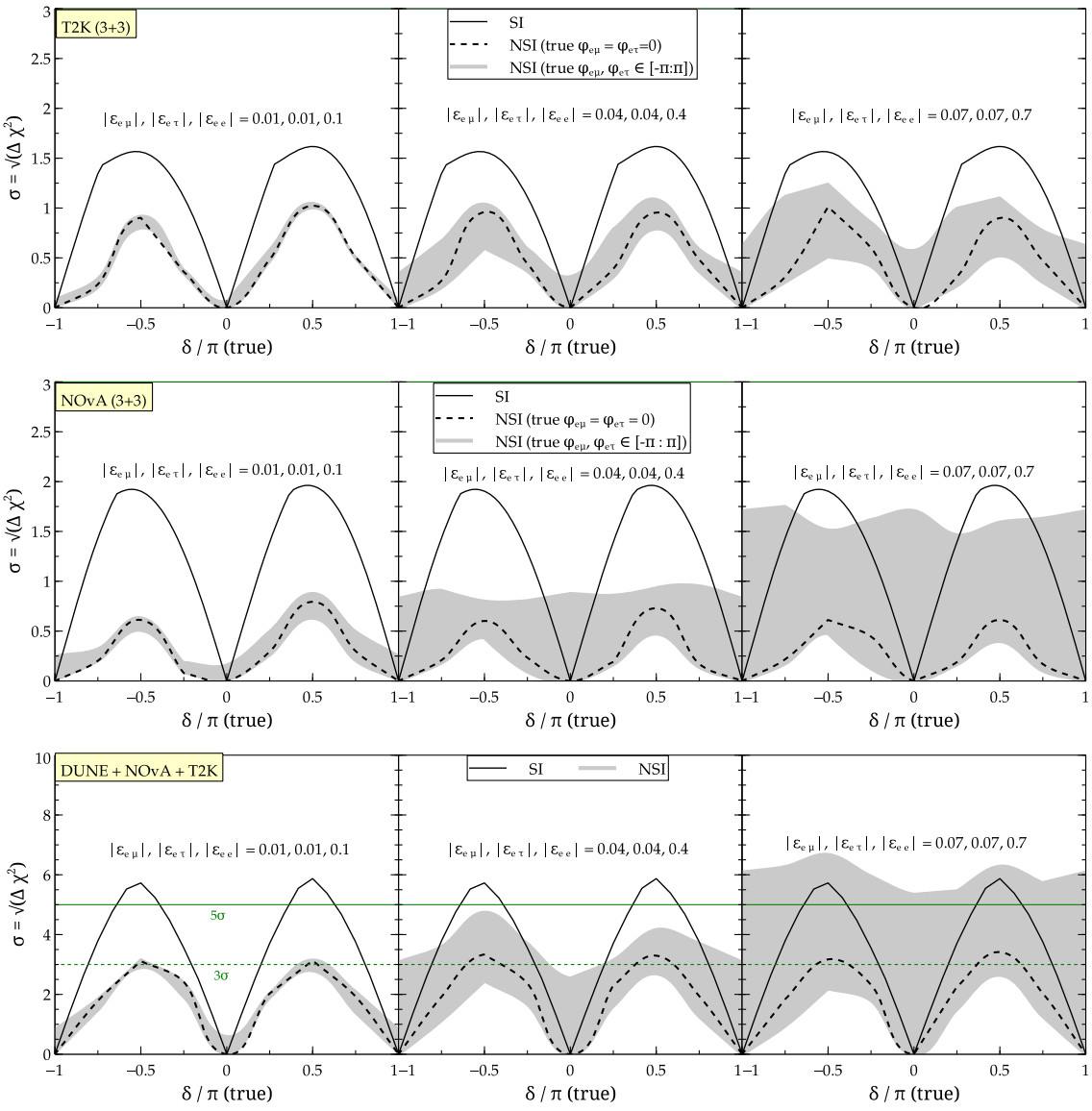


FIG. 8. *CP* violation sensitivity at T2K, NO$\nu$A, and T2K + NO$\nu$A + DUNE for the collective NSI case and SI as a function of true $\delta$.

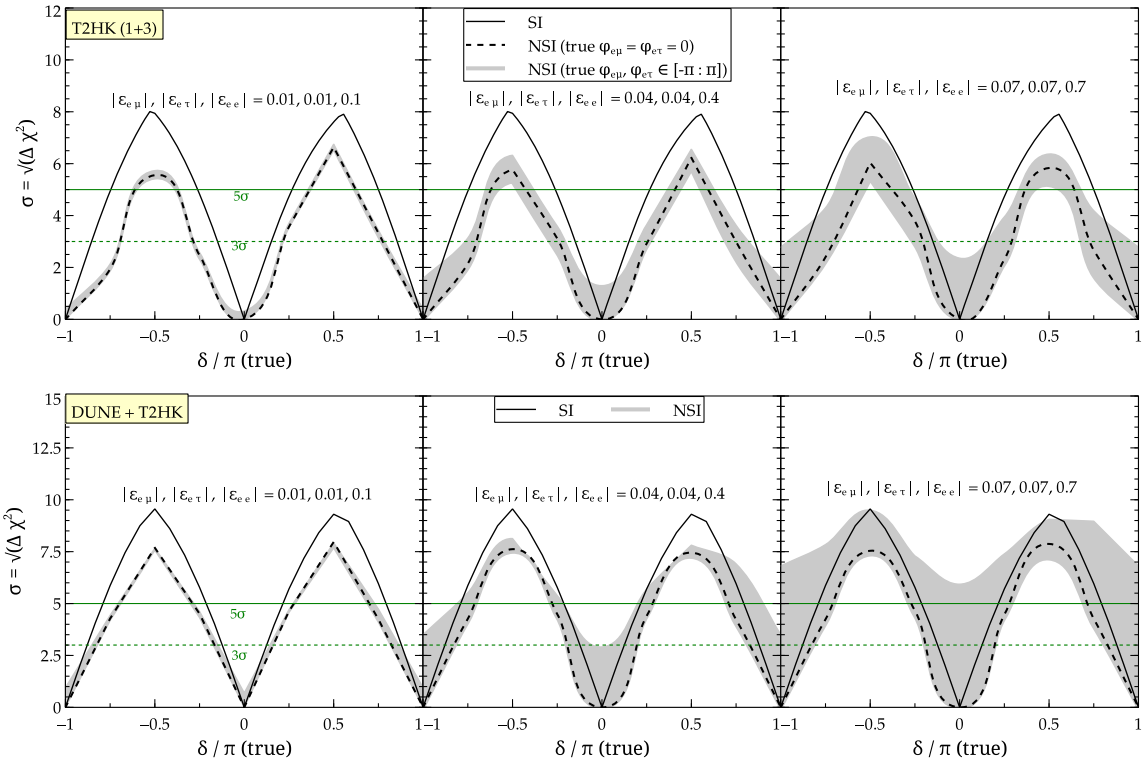


FIG. 9. *CP* violation sensitivity at T2HK and T2HK + DUNE for collective the NSI case and SI as a function of true $\delta$.

means that there is no clear demarcation of *CP*-conserving ($\delta = 0, \pm\pi$) and *CP*-violating values of $\delta$.

In Fig. 9, we show the *CP* violation sensitivity for T2HK. We note that T2HK offers *CP* sensitivity that is competitive with DUNE individually as well as T2K, NO$\nu$A, and DUNE combined (SI and NSI both). This can be ascribed to the high statistics offered by the HK. Near the peak, we note that it can go up to $\sim 8\sigma$ for SI and $\gtrsim 5\sigma$ for NSI (zero phases). Another intriguing feature from the T2HK panel is that the NSI phases do not have as dramatic effect as seen for DUNE when the NSI terms are large—this can be seen as shrinking of the grey regions in Fig. 9 (top panel, rightmost plot). This is due to the fact that the baseline of 295 km is way too short for matter effects (SI and NSI both) to develop and play a significant role.[11] This demonstrates the complementarity of bigger detectors (T2HK) vis-a-vis the long baselines involved (DUNE) where no clear demarcation of *CP*-conserving ($\delta = 0, \pm\pi$) and *CP*-violating values of $\delta$ was noticed.

### D. Optimal exposure for *CP* violation discovery

The previous set of plots was obtained by keeping the total exposure fixed for a given experimental configuration. The maximum value of $f(\sigma > 3)$ guides the choice of optimal exposure for *CP* violation discovery. Let us see how the choice of optimal exposure in the case of SIs is arrived at. We have already noted that the *CP* violation sensitivity as a function of $\delta$ has a double peak structure for SIs due to the vanishing of the sensitivity at *CP*-conserving values of $\delta$ ($= 0, \pm\pi$). Therefore, it is expected that none of the experiments considered in the present work can lead to a 100% coverage in $\delta$ in the SI case. This no longer holds in the presence of NSI.

In Fig. 10, we show the *CP* fraction for which the sensitivity to *CP* violation exceeds $3\sigma$ as a function of exposure, labeled as $f(\sigma > 3)$. Let us first understand the SI case; we note that $f(\sigma > 3)$ rises from 0 to $\sim$0.4 as a function of exposure initially as we go from 50–150 kt. MW. yr but saturates to a value $f(\sigma > 3) \simeq 0.5$–$0.55$ as we go to exposures beyond $\sim$350 kt MW yr. Increasing the exposure further does not change this value drastically beyond $f(\sigma > 3) \simeq 0.5$. This is not unexpected as we have already noticed that it is challenging to exclude those values of the *CP* phase which lie close to the *CP*-conserving values (i.e., 0 and $\pi$). So, in the case of SIs, the choice of optimal exposure is expected to be $\simeq$350 kt MW yr.

Let us now discuss the impact of NSI on the choice of the optimal exposure. For the NSI case, the three panels in Fig. 10 correspond to the three different NSI terms (taken in isolation). There are three colored regions (blue, green, red) for the off-diagonal NSI terms which correspond to the three values of moduli of NSI parameters along with their

[11]Similar features can also be seen from the T2K panel in Fig. 8.

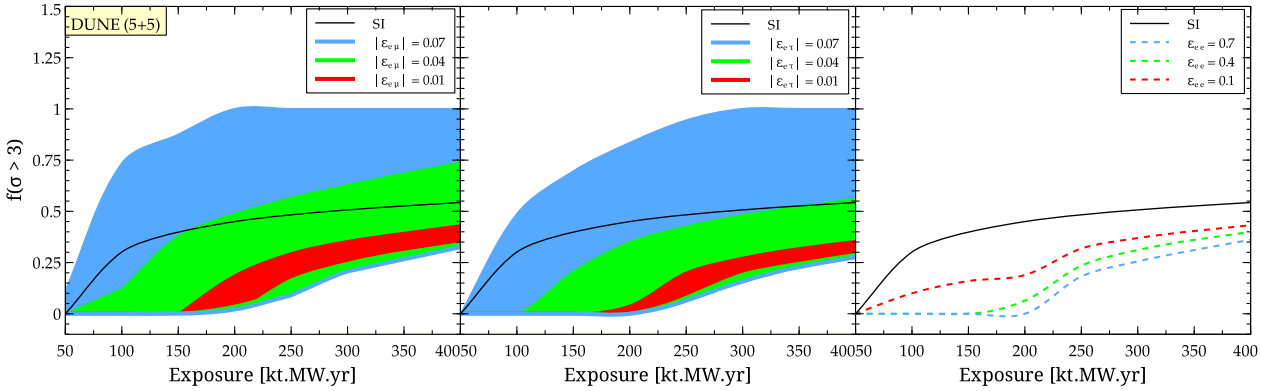


FIG. 10. The *CP* fraction $f(\sigma > 3)$ for which the sensitivity to *CP* violation is greater than $3\sigma$ as a function of exposure for the SI and NSI cases assuming NH. The three plots correspond to three different NSI parameters taken one at a time with full phase variation. The red, green, and blue shaded regions correspond to different values of $\varepsilon_{e\mu}$ and $\varepsilon_{e\tau}$.

respective phase variation (analogous to the grey bands seen in Figs. 3 and 4). For the diagonal NSI terms, there are three dashed lines (blue, green, red) corresponding to three different values of the diagonal NSI parameter $\varepsilon_{ee}$ (see Fig. 5). The plot on the left shows the impact of $\varepsilon_{e\mu}$. Even with the phase variation, $f(\sigma > 3)$ (shown as red band) remains below the SI curve for the small value of $\varepsilon_{e\mu}$ ($|\varepsilon_{e\mu}| = 0.01$). This is due to the dominating statistical effect (a) mentioned in Sec. III A. $f(\sigma > 3)$ stays at zero and does not rise until an exposure of $\simeq$150 kt MW yr is reached. Finally, it attains a value in the range $\simeq$0.35–0.45 as we reach exposures $\sim$400 kt MW yr. For intermediate and large values of $\varepsilon_{e\mu}$ ($|\varepsilon_{e\mu}| = 0.04,\ 0.07$) on the other hand, $f(\sigma > 3)$ gets distributed over a larger range of values for some favorable choice of parameters [due to the interplay of (a) and (b) mentioned in Sec. III A] as can be seen from the green and blue bands. Incorporating the phase variation of the NSI parameter leads to an increase in the value of $f(\sigma > 3)$ and it can reach $\sim$1 when the exposure is barely 200 kt. MW. yr (for some choice of phases, some part of the grey band is above the $3\sigma$ line in Figs. 3 and 4 for all true values of $\delta$). Similar effects are seen for the other off-diagonal parameter, $\varepsilon_{e\tau}$ which is shown in the middle panel. However, for the diagonal NSI parameter $\varepsilon_{ee}$ (which is real), we note that the $f(\sigma > 3)$ (blue, green, and red dashed lines) is always smaller than in the SI case for a given choice of systematics (see also Fig. 5). This is again due to the statistical effect.

We have checked that if we take the true hierarchy as inverted hierarchy (IH) instead of NH, the impact of NSI shown in Fig. 10 is grossly the same (see Table IV). The impact of individual NSI terms on the value of $f(\sigma > 3)$ at an exposure of 350 kt. MW. yr (which is the optimal choice for SI) at DUNE is listed in Table IV for NH and IH.

### E. Role of systematics

The impact of different assumptions on systematics can be seen in Fig. 11. The nominal set of systematics is mentioned in Table II. The black solid curve represents our nominal choice of systematics given in Table II while the blue solid curve is for an optimal choice mentioned in the legend [10]. The green (magenta) band corresponds to NSI case for off-diagonal parameters $\varepsilon_{e\mu}$, $\varepsilon_{e\tau}$ with full phase variation for a nominal (optimal) choice of systematics. The green (magenta) dashed curve is for $\varepsilon_{ee}$ for a nominal (optimal) choice of systematics.

It can be seen that $f(\sigma > 3)$ nearly reaches its maximum ($\sim$0.55) possible value at around 1300 km for SI (see Fig. 11). This implies that for the given configuration of the far detector planned for DUNE (see Table II), the optimal distance to be able to infer the highest fraction of the values of the *CP* phase is $\sim$1300 km. Clearly, even in case of SI, better systematics is expected to lead to a larger $f(\sigma > 3)$ for a given baseline, say at 1300 km—it changes from $\sim$0.55 to $\sim$0.71. For the SI case, better systematics ensures better detectability of *CP* violation quantified in terms of fraction $f(\sigma > 3)$ and at the same time, does not alter the optimal baseline choice for the *CP* violation

TABLE IV. $f(\sigma > 3)$ at an exposure of 350 kt. MW. yr for DUNE using nominal systematics (see Fig. 10).

| | NH | | IH | |
|---|---|---|---|---|
| NSI term | $f(\sigma > 3)$ (NSI) | $f(\sigma > 3)$ (SI) | $f(\sigma > 3)$ (NSI) | $f(\sigma > 3)$ (SI) |
| $\lvert\varepsilon_{e\mu}\rvert = 0.01$ | 0.32–0.40 | 0.52 | 0.35–0.42 | 0.58 |
| $\lvert\varepsilon_{e\mu}\rvert = 0.04$ | 0.30–0.69 | 0.52 | 0.33–0.78 | 0.58 |
| $\lvert\varepsilon_{e\mu}\rvert = 0.07$ | 0.27–1.00 | 0.52 | 0.32–1.00 | 0.58 |
| $\lvert\varepsilon_{e\tau}\rvert = 0.01$ | 0.26–0.32 | 0.52 | 0.23–0.32 | 0.58 |
| $\lvert\varepsilon_{e\tau}\rvert = 0.04$ | 0.24–0.53 | 0.52 | 0.22–0.84 | 0.58 |
| $\lvert\varepsilon_{e\tau}\rvert = 0.07$ | 0.23–1.00 | 0.52 | 0.21–1.00 | 0.58 |
| $\varepsilon_{ee} = 0.01$ | 0.40 | 0.52 | 0.36 | 0.58 |
| $\varepsilon_{ee} = 0.04$ | 0.36 | 0.52 | 0.30 | 0.58 |
| $\varepsilon_{ee} = 0.07$ | 0.31 | 0.52 | 0.27 | 0.58 |

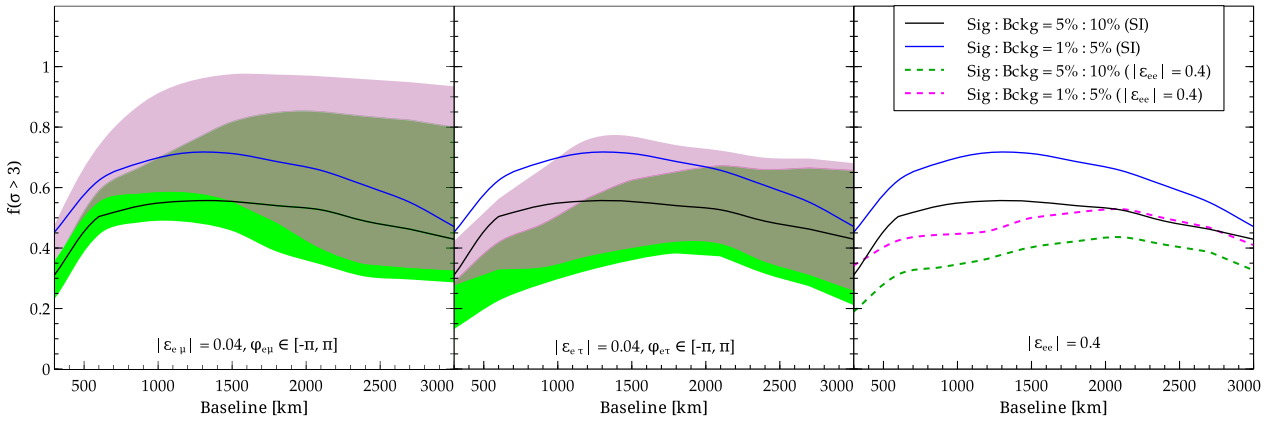


FIG. 11. The *CP* fraction for which the sensitivity to *CP* violation is greater than $3\sigma$ as a function of the baseline for SI and NSI cases. The black and blue solid curves correspond to the different systematics assumed for SIs. The three plots correspond to three NSI parameters taken one at a time. The green (magenta) band corresponds to the choice of nominal (optimal) systematics with full phase variation for the off-diagonal NSI parameters while the green (magenta) dashed line corresponds to $\varepsilon_{ee}$ for nominal (optimal) systematics.

sensitivity. In the case of NSI, the green (magenta) band show the effect of two choices of systematics and there is an overlap between them as well as with the SI values. These aspects play a crucial role in altering the choice of the best baseline for *CP* violation sensitivity. However, in the presence of NSI, for the choice of NSI phases representing the top (bottom) edge of the green or magenta band (we have used the dashed green or magenta lines to depict the diagonal NSI terms), the optimal choice of baseline ($L_{\rm opt}$) that maximizes the *CP* fraction changes as a function of systematics (see Table V).

### F. *CP* violation sensitivity assuming known source

In the preceding discussion, we assumed that the source of *CP* violation (i.e., whether it arises due to the SI *CP*-violating parameter $\delta$ or due to NSI *CP*-violating parameters $\varphi_{e\mu}$, $\varphi_{e\tau}$) cannot be traced or, in other words, is unknown. If one knows which parameter is responsible for *CP* violation, the results are drastically modified. In order to illustrate this, let us assume that out of the possible sources of *CP* violation, i.e., $\delta$, $\varphi_{e\mu}$ or $\varphi_{e\tau}$, only one of these is responsible at a time for generating *CP*-violating effects. The results for the case of the known source of *CP* violation are depicted in Fig. 12. The three rows correspond to the case when the known source is $\delta$ (top), $\varphi_{e\mu}$ (middle), and $\varphi_{e\tau}$ (bottom). From the top row, we note that the presence of the NSI spoils the *CP* violation sensitivity irrespective of the strength of the NSI terms as compared to the standard case (black solid curves). Also, since $\delta$ is the only source of *CP* violation, in the first row, the *CP* violation sensitivity drops nearly to zero at $\delta = 0, \pm\pi$ for all the three cases shown. This is in sharp contrast with Fig. 6 where all of the phases would have contributed to the *CP* violation sensitivity. The middle and the bottom row correspond to the case when $\varphi_{e\mu}$ and $\varphi_{e\tau}$ are the only sources of *CP* violation. Again the characteristic double peak structure is visible but the *CP* violation sensitivity is not as large as for the top row simply

TABLE V. Maximum $f(\sigma > 3)$ and optimal baseline range ($L_{\rm opt}$) for the two different choices of systematics (see Fig. 11) for NH. The values with larger (smaller) $f(\sigma > 3)$ correspond to upper (lower) edge of the respective bands.

| | Nominal Systematics (Green) | | Optimal Systematics (Magenta) | |
|---|---|---|---|---|
| | NSI | SI | NSI | SI |
| NSI Term | $f(\sigma > 3)$ $L_{\rm opt}$ km | $f(\sigma > 3)$ $L_{\rm opt}$ km | $f(\sigma > 3)$ $L_{\rm opt}$ km | $f(\sigma > 3)$ $L_{\rm opt}$ km |
| $\lvert\varepsilon_{e\mu}\rvert = 0.04$ | 0.85 (1800–2500)<br>0.49 (800–1300) | 0.52 (1300) | 0.97 (1500–3000)<br>0.59 (800–1300) | 0.71 (1300) |
| $\lvert\varepsilon_{e\tau}\rvert = 0.04$ | 0.65 (2000–3000)<br>0.37 (1800–2000) | 0.52 (1300) | 0.77 (1300–1500)<br>0.40 (1800–2000) | 0.71 (1300) |
| $\varepsilon_{ee} = 0.04$ | 0.43 (1900–2100) | 0.52 (1300) | 0.52 (1900–2100) | 0.71 (1300) |

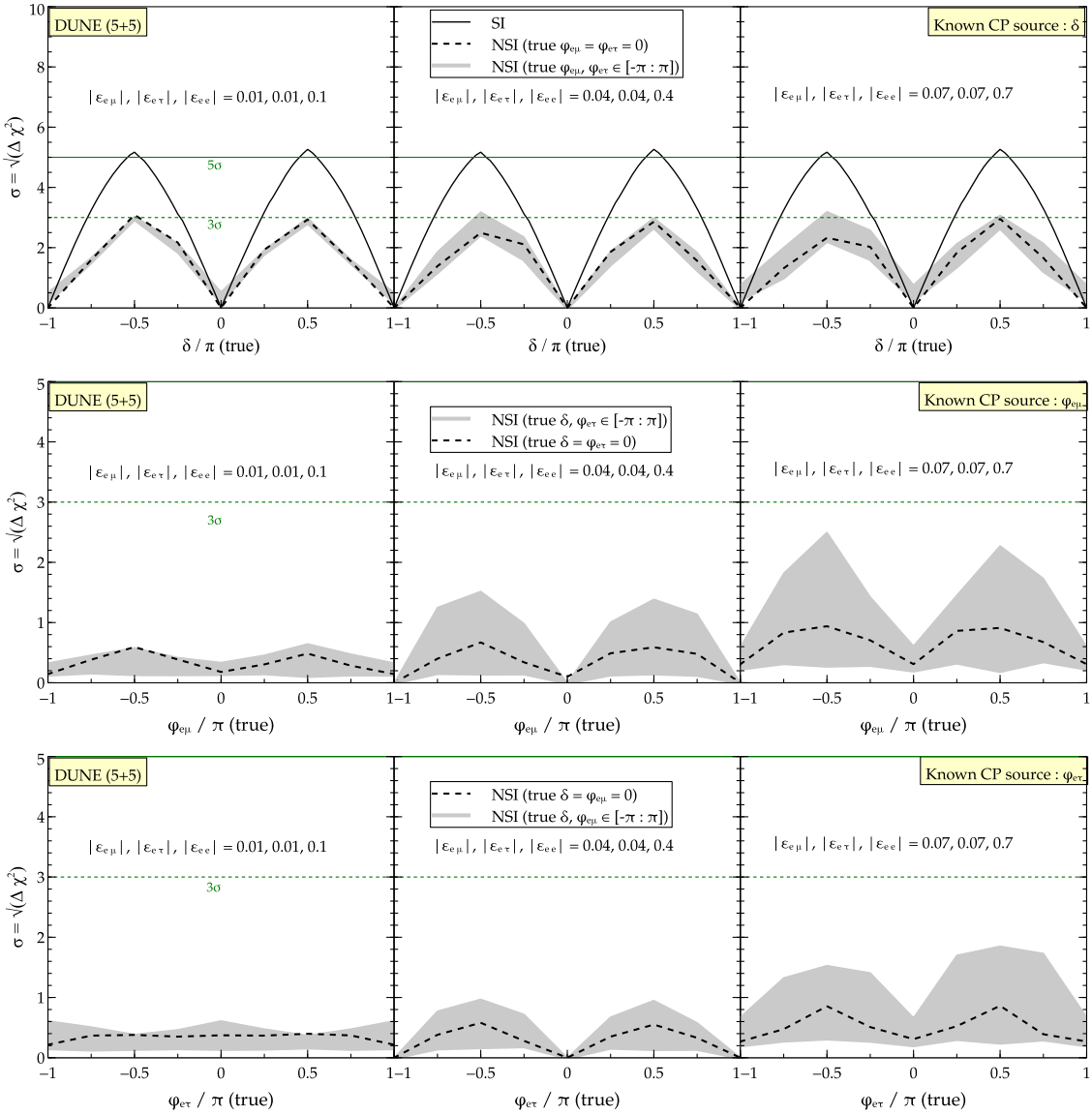


FIG. 12. *CP* violation sensitivity if the source of *CP* violation is known. The three rows correspond to one known source (shown along the $x$ axis) at a time.

because NSI effects are subdominant. For Fig. 12, in the $\chi^2$ evaluation, we marginalize over the full allowed range[12] of the remaining phases (for the case of top row, $\varphi_{e\mu}$, $\varphi_{e\tau}$) in Eq. (13).

### G. Measuring the phases that may be responsible for *CP* violation

Independent of the question of the *CP* violation sensitivity that we have addressed in the present article, one can ask if it is possible to measure the *CP* phases at long baseline experiments. For the sake of simplicity, we assume that only one NSI parameter contributes at a time (let us assume that this is given by $\varphi_{e\mu}$).[13] Let us now take some representative values of the true *CP* phases and discuss how well we are able to reconstruct those values among the allowed test ranges. In Fig. 13, for two possible choices of the pair of phases, $\{\delta^{\text{true}}, \varphi_{e\mu}^{\text{true}}\} = \{\pi/2, \pi/2\}$ (maximal *CP* violation) and $\{\delta^{\text{true}}, \varphi_{e\mu}^{\text{true}}\} = \{0, 0\}$ (*CP* conservation), we show the ability of DUNE to reconstruct those phases assuming NH. For a comparison, we also show the results for the combined case of DUNE + T2HK where

[12]The full allowed range is $[-\pi, \pi]$ in contrast to the *CP*-conserving values $(0, \pi)$ considered in the previous section when the source of *CP* violation was assumed to be unknown. The statistical effect is expected to dominate in this scenario due to the wider ranges considered for the marginalization over the test values of the *CP*-violating parameters.

[13]For the other NSI parameter $\varphi_{e\tau}$, the results are similar.

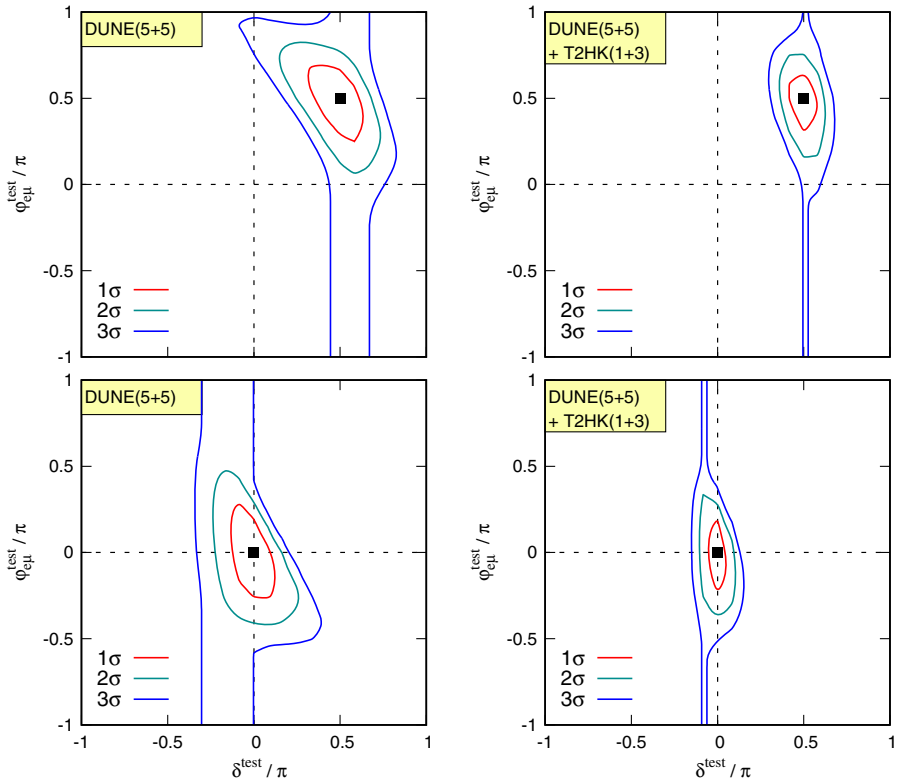


FIG. 13. Regions in the $\varphi_{e\mu}^{test}$–$\delta^{test}$ plane. The black dot represents the pair of true values $\{\varphi_{e\mu}^{true}, \delta^{true}\}$ which are taken to be $\{\pi/2, \pi/2\}$ (*CP* violating) in the top row or $\{0, 0\}$ (*CP* conserving) in the bottom row. The value of the NSI parameter is taken to be $|\varepsilon_{e\mu}| = 0.04$. The plots on the left are for DUNE and those on the right are for DUNE + T2HK.

we see that the regions enclosed by the contours become narrower.

The region outside the $3\sigma$ contour represents those values of the pair of test *CP* phases which can be safely discarded above $3\sigma$ while reconstructing their values for the specific choice of the true pair of *CP* phases. Smaller enclosed regions by the contours (see Fig. 13, right panel) imply better measurement ability. Let us

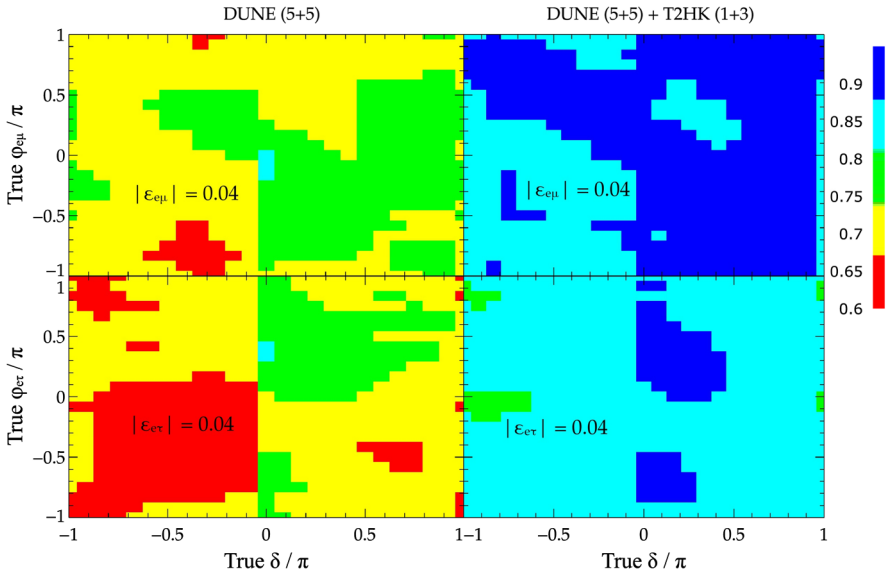


FIG. 14. Oscillograms of the generalized *CP* fraction in $\varphi_{e\mu}^{true}$–$\delta^{true}$ plane.

define a generalized $CP$ fraction at a given confidence level[14] as the ratio of the area outside the contours to the full area. This quantity allows us to have an idea of how well a pair of $CP$ phases can be reconstructed at any given confidence level. The large $CP$ fraction implies better identification of the $CP$ pair among the test values.

To take into account all possible choices of the true pair of $CP$ phases, we show in Fig. 14 oscillograms of the generalized $CP$ fraction in the $\varphi_{e\mu}^{\text{true}} - \delta^{\text{true}}$ and $\varphi_{e\tau}^{\text{true}} - \delta^{\text{true}}$ planes. The colors represent values of the generalized $CP$ fraction in the range 0.6–1. For the case of DUNE, the range of the generalized $CP$ fraction is $\simeq$0.6–0.8 while if we add T2HK to DUNE, the range of $CP$ fraction becomes $\simeq$0.85–1. This means that T2HK when combined with DUNE allows us to measure the $CP$ phases much better.

## IV. DISCUSSION AND CONCLUSION

With tremendous progress on both theoretical and experimental fronts in neutrino oscillation physics, we have a fairly good idea of the neutrino masses and mixing pattern. The proposed long baseline experiment, DUNE, aims to hunt for the most sought after parameter, the $CP$-violating phase $\delta$. In the era of precision, the subdominant effects due to new physics, such as NSIs, need to be incorporated carefully. We have discussed the impact of propagation NSIs on the standard procedure to determine the $CP$ violation sensitivity at long baseline experiments. The impact of NSIs (including new $CP$ phases) on the $CP$ measurements at DUNE using only the appearance channel was studied analytically as well as numerically at the level of probability and event rates in Ref. [36]. In the present article, we perform a full-fledged sensitivity analysis using appearance and disappearance channels and quantify the effects at the level of $\chi^2$ and the $CP$ fraction $f(\sigma > 3)$. We considered the NSI terms individually first and then a combination of the dominant ones. We also compare the $CP$ sensitivities with other ongoing experiments—T2K, NO$\nu$A and a future generation experiment—T2HK.

We have found a general rule (in Sec. III A) that allows us to comprehend the results very nicely. There are two opposing effects at work—one is purely statistical which tends to decrease the $CP$ sensitivity while the other one is due to the variation of the true values of the additional $CP$ phases which tends to broaden the sensitivity bands provided the true value of the modulus of the relevant NSI parameter is large. For diagonal NSI terms, only the first effect dominates while for the off-diagonal NSI terms, the additional $CP$ phases may enhance or lower the sensitivity to $CP$ violation thereby broadening the grey bands as well as increasing the value of the $CP$ fraction depending on the strength of the NSI term. We would like to stress that although the value of $\chi^2$ in the presence of NSI may sometimes be greater than the SI case [due to effect (b)], this is not to be interpreted in a positive sense, i.e., this does not mean that the sensitivity to the violation of the Dirac $CP$ phase has necessarily increased. Rather it illustrates that in the presence of new sources of $CP$ violation (NSI moduli and phases), the sensitivity to the standard Dirac $CP$ violation has been compromised in a very significant way.

It is shown that DUNE is sensitive not only to $CP$ violation effects due to the genuine SI $CP$ phase [10] but also to additional (fake and genuine) $CP$-violating effects arising due to moduli and phases of the NSI parameters. Finally, we can infer the following:

(i) The NSI parameters $\varepsilon_{e\mu}$, $\varepsilon_{e\tau}$, and $\varepsilon_{ee}$ show the largest effect in the $P_{\mu e}$ channel. While the NSI parameters $\varepsilon_{\mu\tau}$, $\varepsilon_{\mu\mu}$, and $\varepsilon_{\tau\tau}$ are expected to contribute to the $P_{\mu\mu}$ channel, we do not consider them here because the disappearance channel by itself contributes very little to the $CP$ sensitivity owing to the absence of $CP$-odd terms in the probability. Even if we consider these parameters, we find that the $\varepsilon_{\mu\mu}$ is constrained very strongly [Eq. (9)]. We have checked the impact of $\varepsilon_{\mu\tau}$ on the $CP$ violation sensitivity using both appearance and disappearance channels and it is found to be negligible for DUNE. The effect of $\varepsilon_{\tau\tau}$ is shown in Fig. 5 and is smaller in comparison to $\varepsilon_{ee}$. For these reasons, we consider $\varepsilon_{e\mu}$, $\varepsilon_{e\tau}$, and $\varepsilon_{ee}$ as the dominant NSI parameters affecting $CP$ sensitivity.

(ii) The dependence of $CP$ sensitivity on the true values of $\theta_{23}$ and $\delta m^2_{31}$ is depicted in Fig. 7. While $\theta_{23}$ changes the sensitivity both for SIs and NSIs, the $\delta m^2_{31}$ has minuscule effect. Since $\theta_{13}$ is measured very precisely [47], we do not expect any change due to the effect of variation of the true value of $\theta_{13}$.

(iii) We also compared the expected sensitivity of DUNE with current long baseline experiments T2K, NO$\nu$A and a future experiment, T2HK. The long baseline experiments—T2K and NO$\nu$A are not useful from the point of view of $CP$ sensitivity both in SIs and NSIs when considered in isolation but adding data to DUNE can lead to an increase in sensitivity. In spite of the short baseline of the future T2HK experiment, the high statistics leads to sensitivity that is comparable to that obtained with the longer baseline experiment, DUNE. It is suggested [38] that a combination of DUNE and T2HK may be able to improve constraints on some of the NSI parameters and may also be able to resolve degeneracies.

(iv) The impact of NSI on the $CP$ fraction for which sensitivity to $CP$ violation is greater than $3\sigma$ at DUNE as a function of exposure is shown in Fig. 10. For smaller values of the off-diagonal NSI terms, we note

[14]This is different from the $CP$ fraction that we have introduced earlier which involves only the Dirac $CP$ phase ($\delta$).

that the bands are always below the black solid curve for SIs. As we increase the value, the bands spread on either side of the black curve. For the diagonal NSI parameter $\varepsilon_{ee}$ the curve due to NSI is always below the black curve for the values considered here. Table IV summarizes the change in thevalue of $f(\sigma > 3)$ compared to the SI case for nominal systematics at an optimal exposure of 350 kt. MW. yr in case of DUNE for both NH and IH.

(v) The impact of change in systematics as a function of baseline is shown in Fig. 11 and Table V. It is shown that the choice of optimal baseline changes when we include effects due to NSI.

(vi) If the source of *CP* violation is exactly known then the *CP* violation sensitivity in the presence of NSI is always dominated by effect (a) as discussed in Sec. III F. The results are shown in Fig. 12 as a function of the three different phases involved.

(vii) The ability of long baseline experiments to measure the value of standard or nonstandard *CP* phases is discussed in Sec. III G and shown in Figs. 13 and 14. Adding T2HK to DUNE helps in increasing the value of the generalized *CP* fraction which in turn implies that measurement of the *CP* phases will be far better.

We therefore conclude that new physics effects such as propagation NSI spoil the *CP* sensitivity at long baseline neutrino experiments, in general, and specifically in the context of DUNE. This spoiling can be in either direction depending upon the strength of the NSI terms involved. The problem then reduces to disentangling standard *CP* violation from the nonstandard *CP* violation.

Another observation that can be made from this study is that if $f(\sigma > 3)$ such that $f(\sigma > 3) \sim 1$ (for shorter exposures) and significantly larger than its value for the given systematics, then it unequivocally implies that there is new physics giving rise to it. Then the task is to find the new physics scenario uniquely that could give rise to such a large value. However if $f(\sigma > 3)$ stays far from unity for reasonable exposures then we can constrain the NSI terms very well using long baseline experiments such as DUNE.

If we look at different experiments, naturally the impact of NSI will be less for the relatively shorter baselines since the amount of matter traversed will be less. So, T2K and T2HK experience a lesser impact than NO$\nu$A and DUNE. For shorter baselines such as 295 km, the characteristic double peak structure of the *CP* sensitivity curve as a function of true $\delta$ survives and there is clear distinction between the *CP*-conserving and *CP*-violating cases. T2HK due to the shorter baseline and high statistics does better in demarcating the *CP*-conserving and *CP*-violating values as the grey bands are not so broad. However, for longer baselines such as for NO$\nu$A and DUNE, the *CP* sensitivity as a function of $\delta$ flattens out for some choice of phases of the relevant NSI parameters (upper edge of the grey band). This poses a problem in differentiating the *CP*-conserving and *CP*-violating cases. In effect, this can mask/obscure the measurement of the SI *CP* phase, if the nature had it to be *CP* conserving. For favorable values of the *CP* phase (near $\pm\pi/2$), DUNE will be competitive with T2HK. But, if *CP* phases were in the unfavorable region (near $\sim 0, \pi$), then the future T2HK experiment will be very promising.

## ACKNOWLEDGMENTS

It is a pleasure to thank Raj Gandhi for useful discussions and critical comments on the manuscript. We acknowledge the use of HRI cluster facility to carry out computations in this work. P. M. acknowledges support from University Grants Commission under the second phase of University with Potential of Excellence at JNU and partial support from the European Union Grant No. FP7 ITN INVISIBLES (Marie Curie Actions, PITN-GA-2011-289442). We thank the organizers of WHEPP at IIT-Kanpur for the warm hospitality where substantial progress in the work was carried out. We are grateful to the anonymous referee for constructive suggestions and inputs.

[1] L. Wolfenstein, Phys. Rev. Lett. **13**, 562 (1964).
[2] G. C. Branco, R. G. Felipe, and F. R. Joaquim, Rev. Mod. Phys. **84**, 515 (2012).
[3] M. Kobayashi and T. Maskawa, Prog. Theor. Phys. **49**, 652 (1973).
[4] V. D. Barger, K. Whisnant, and R. J. N. Phillips, Phys. Rev. Lett. **45**, 2084 (1980).
[5] H. Nunokawa, S. J. Parke, and J. W. F. Valle, Prog. Part. Nucl. Phys. **60**, 338 (2008).
[6] Y. Farzan and A. Yu. Smirnov, J. High Energy Phys. 01 (2007) 059.
[7] J. Arafune, M. Koike, and J. Sato, Phys. Rev. D **56**, 3093 (1997), **60**, 119905(E) (1999).
[8] T. Ohlsson, H. Zhang, and S. Zhou, Phys. Rev. D **87**, 053006 (2013).
[9] W. Marciano and Z. Parsa, Nucl. Phys. B, Proc. Suppl. **221**, 166 (2011).
[10] M. Bass *et al.* (LBNE Collaboration), Phys. Rev. D **91**, 052015 (2015).
[11] R. Acciarri *et al.* (DUNE Collaboration), arXiv:1512.06148.
[12] R. Acciarri *et al.* (DUNE Collaboration), arXiv:1601.02984.
[13] R. Acciarri *et al.* (DUNE Collaboration), arXiv:1601.05471.

[14] X. Qian and P. Vogel, Prog. Part. Nucl. Phys. **83**, 1 (2015).
[15] V. Barger, A. Bhattacharya, A. Chatterjee, R. Gandhi, D. Marfatia, and M. Masud, Phys. Rev. D **89**, 011302 (2014).
[16] V. Barger, A. Bhattacharya, A. Chatterjee, R. Gandhi, D. Marfatia, and M. Masud, Int. J. Mod. Phys. A **31**, 1650020 (2016).
[17] M. Ghosh, S. Goswami, and S. K. Raut, Eur. Phys. J. C **76**, 114 (2016).
[18] K. Abe *et al.* (Hyper-Kamiokande Proto-Collaboration), Prog. Theor. Exp. Phys. **2015**, 053C02 (2015).
[19] M. Blennow, P. Coloma, and E. Fernández-Martinez, J. High Energy Phys. 03 (2016) 197.
[20] Y. Farzan, Phys. Lett. B **748**, 311 (2015).
[21] Y. Farzan and I. M. Shoemaker, J. High Energy Phys. 07 (2016) 033.
[22] M. C. Gonzalez-Garcia, Y. Grossman, A. Gusso, and Y. Nir, Phys. Rev. D **64**, 096006 (2001).
[23] W. Winter, Phys. Lett. B **671**, 77 (2009).
[24] A. Chatterjee, P. Mehta, D. Choudhury, and R. Gandhi, Phys. Rev. D **93**, 093017 (2016).
[25] D. V. Forero, M. Tortola, and J. W. F. Valle, Phys. Rev. D **90**, 093006 (2014).
[26] K. Abe *et al.* (T2K Collaboration), Phys. Rev. D **91**, 072010 (2015).
[27] P. Adamson *et al.* (vA Collaboration), Phys. Rev. Lett. **116**, 151806 (2016).
[28] C. Kachulis, https://indico.cern.ch/event/361123/session/2/contribution/348/attachments/1136004/1625868/SK_atmospheric_kachulis_dpf2015.pdf.
[29] D. V. Forero and P. Huber, Phys. Rev. Lett. **117**, 031801 (2016).
[30] T. Ohlsson, Rep. Prog. Phys. **76**, 044201 (2013).
[31] O. G. Miranda and H. Nunokawa, New J. Phys. **17**, 095002 (2015).
[32] A. Datta, R. Gandhi, P. Mehta, and S. U. Sankar, Phys. Lett. B **597**, 356 (2004).
[33] A. Chatterjee, R. Gandhi, and J. Singh, J. High Energy Phys. 06 (2014) 045.
[34] R. Gandhi, B. Kayser, M. Masud, and S. Prakash, J. High Energy Phys. 11 (2015) 039.
[35] J. M. Berryman, A. de Gouva, K. J. Kelly, and A. Kobach, Phys. Rev. D **92**, 073012 (2015).
[36] M. Masud, A. Chatterjee, and P. Mehta, arXiv:1510.08261 [J. Phys. G (to be published)].
[37] A. Friedland and I. M. Shoemaker, arXiv:1207.6642.
[38] P. Coloma, J. High Energy Phys. 03 (2016) 016.
[39] A. de Gouvea and K. J. Kelly, Nucl. Phys. **B908**, 318 (2016).
[40] J. Liao, D. Marfatia, and K. Whisnant, Phys. Rev. D **93**, 093016 (2016).
[41] K. Huitu, T. J. Kärkkäinen, J. Maalampi, and S. Vihonen, Phys. Rev. D **93**, 053016 (2016).
[42] P. Bakhti and Y. Farzan, arXiv:1602.07099.
[43] J. Beringer *et al.* (Particle Data Group), Phys. Rev. D **86**, 010001 (2012).
[44] P. Mehta, Phys. Rev. D **79**, 096013 (2009).
[45] P. Mehta, arXiv:0907.0562.
[46] T. Kikuchi, H. Minakata, and S. Uchinami, J. High Energy Phys. 03 (2009) 114.
[47] M. C. Gonzalez-Garcia, M. Maltoni, and T. Schwetz, J. High Energy Phys. 11 (2014) 052.
[48] P. Huber, M. Lindner, and W. Winter, Comput. Phys. Commun. **167**, 195 (2005).
[49] J. Kopp, Int. J. Mod. Phys. C **19**, 523 (2008).
[50] P. Huber, J. Kopp, M. Lindner, M. Rolinec, and W. Winter, Comput. Phys. Commun. **177**, 432 (2007).
[51] J. Kopp, M. Lindner, T. Ota, and J. Sato, Phys. Rev. D **77**, 013007 (2008).
[52] A. M. Dziewonski and D. L. Anderson, Phys. Earth Planet. Inter. **25**, 297 (1981).
[53] R. Gandhi, P. Ghoshal, S. Goswami, P. Mehta, and S. U. Sankar, Phys. Rev. Lett. **94**, 051801 (2005).
[54] R. Gandhi, P. Ghoshal, S. Goswami, P. Mehta, and S. U. Sankar, Phys. Rev. D **73**, 053001 (2006).
[55] M. Gonzalez-Garcia, M. Maltoni, J. Salvado, and T. Schwetz, J. High Energy Phys. 12 (2012) 123.
[56] F. Capozzi, G. L. Fogli, E. Lisi, A. Marrone, D. Montanino, and A. Palazzo, Phys. Rev. D **89**, 093018 (2014).
[57] K. Kimura, A. Takamura, and H. Yokomakura, Phys. Lett. B **537**, 86 (2002).
[58] K. Kimura, A. Takamura, and H. Yokomakura, Phys. Rev. D **66**, 073005 (2002).
[59] O. Yasuda, arXiv:0704.1531.
[60] D. Meloni, T. Ohlsson, and H. Zhang, J. High Energy Phys. 04 (2009) 033.
[61] V. Barger, D. Marfatia, and K. Whisnant, Phys. Rev. D **65**, 073023 (2002).
[62] X. Qian, A. Tan, W. Wang, J. J. Ling, R. D. McKeown, and C. Zhang, Phys. Rev. D **86**, 113011 (2012).